Characterization of $K_v\beta$ Subunit Substrates and Catalysis in the Context of Sleep Regulation

Patrick Ziyun Liu

Magdalen College

Thesis for Doctor of Philosophy in Physiology, Anatomy and Genetics at the University of Oxford

July 14, 2022

Table of contents

Acknowledgements 4

Abstract 6

Introduction 8

Neural and molecular mechanisms of sleep regulation in *Drosophila* 8

K_v subunits and their role in sleep regulation 17

$K_v\beta$ subunit substrates and catalysis in sleep regulation 20

Methods 26

Results chapter 1: Mass spectrometry (MS) characterization of $K_v\beta2$ native ligands 35

Introduction 35

Verification and purification of $K_v\beta2$ construct 37

Purified $K_v\beta2$ is a functional enzyme predominantly bound to NADPH 40

Native MS reveals additional masses bound to $K_v\beta2$ 42

Small molecular weights detected on $K_v\beta2$ 42

POVPC does not stably bind to $K_v\beta2$ 44

Dissociated $K_v\beta2$ from the $K_v1.2$-$K_v\beta2$ complex has additional masses 44

Discussion 48

Results chapter 2: $K_v\beta2$'s influence on A-type current inactivation 52

Introduction 52

$K_v\beta2$ relocates to the plasma membrane in the presence of $K_v1.4$ 54

4-ONE partially prevents $K_v1.4$ inactivation 54

A $K_v1.4$ C13S mutation abolishes 4-ONE's effect on $K_v1.4$ 56

$K_v\beta2$ shields $K_v1.4$ from 4-ONE's partial lack of inactivation effect 57

$K_v\beta2$ delays A-type current inactivation in a substrate-specific manner 57

Membrane depolarization leads to decreased inactivation time constants 60

Discussion 62

Results chapter 3: Altering sleep profiles through manipulating Hyperkinetic's cofactor exchange rate 67

Introduction 67

Native genomic Hyperkinetic expression is detectable in the dFB 68

Designing Hyperkinetic mutants for sleep analysis 70

Increased Hyperkinetic cofactor exchange rate leads to partial sleep rescue 70

Discussion 72

Discussion and Future Directions 76

POVPC reduction and binding 76

Endogenous expression of K_v subunits in HEK-293 cells 77

4-ONE leads to a partial lack of inactivation for $K_v1.4$ 80

Voltage-dependent cofactor exchange 81

Differential Hyperkinetic expression in the dFB 83

Hyperkinetic mutants differentially rescue an insomniac phenotype 85

References 88

Acknowledgements

This thesis would not be possible without the generous support and help from too many individuals to list here, but for whom I am deeply grateful. First and foremost, I am thankful for Professor Gero Miesenböck for being an excellent mentor and welcoming me into his lab as a young scientist eager to learn more about neuroscience. I will never forget when he responded to my initial email asking to join his lab. I am also thankful for Professor Dame Carol Robinson, my secondary supervisor, for allowing me to work so closely with her lab on a fruitful collaboration and to learn so much about mass spectrometry techniques. I am thankful for Siyun Chen, Dinesh Chinthapalli, and Di Wu—member of the Robinson group—for all their time and effort put into our collaboration. I am also thankful for Professor Oleg Fedorov for allowing me to work in his laboratory to learn new techniques, and for Thomas Christott for experimental assistance and helpful discussions.

I am thankful for the entire Miesenböck lab for their generous assistance with techniques and helpful discussions. Within the Miesenböck lab, I am thankful for Paul Volkmann, Jan Kropf, Olof Rorsman, and Clara Besserer for all the help with electrophysiology. I am thankful for Katerina Christodoulou, Olof Rorsman, Celina Hartmann, Lea Ballenberger, Timothy Wong, Alina Krebbers, Anissa Kempf, and Laura Garmendia Sanchez for helping me learn *Drosophila* husbandry. I am thankful for Haram Park, Yeonsoo Choi, Zelie Britton, Ruth Brain, and Raffaele Sarnataro for assistance with cell culture and biochemistry. I am also thankful for Giacomo Bertuzzi, Peter Hasenhuetl, Susanne Szydlowski, Clifford Talbot, Eleftheria Vrontou, and Bohan

Zhao for helpful discussions and support. Last but not least, I am thankful for Fiona Woods for all the assistance with placing orders and arranging logistics.

I am thankful for the Marshall Scholarship for funding my degree program and for allowing me to meet many inspiring peers along the way, and for the University of Pennsylvania Perelman School of Medicine for allowing me to defer my position in their medical class to pursue this wonderful opportunity. At Oxford, I am thankful for Dr. Miriam Chung for all her care and support over the years.

I am thankful for Mr. Aurin for sparking my passion for biology in high school, Cassidy Wang for helping develop my interests in genetics and physiology, Professor Robin Nusslock for inspiring me to go into neuroscience in college, Professor John Marko and Professor Andrew Stephens for training me as a college student, and of course, my parents for making all of this possible.

I owe a great debt to those listed here as well as to many other individuals. Thank you all so much.

Abstract

Better understanding the molecular underpinnings of sleep regulation would provide more insight into the benefits and functions of sleep. The molecular changes underlying sleep and wake are reflected in the electrical excitability of the dorsal fan-shaped body (dFB), a sleep-inducing circuit in *Drosophila melanogaster*. Within the dFB, Hyperkinetic, a $K_v\beta$ subunit of the ion channel Shaker, links increased reactive oxygen species levels to sleep via its oxidoreductase activity and modulatory effects on Shaker's A-type currents. This raises the possibility that Hyperkinetic substrates can influence sleep. However, the endogenous substrates of $K_v\beta$ subunits remain unknown, and proper $K_v\beta$ subunit characterization linking its biochemical properties to sleep remain lacking.

In my thesis, I have established an expression system for mammalian $K_v\beta2$ or the $K_v1.4$-$K_v\beta2$ channel complex in HEK-293 cells and used the recombinant protein as a bait for the detection of endogenous binding partners. I have found that $K_v\beta2$ predominantly binds NADPH, demonstrated its catalytic activity, and identified the masses of several endogenous ligands that may be lipid peroxidation products. Through voltage clamp recordings, I have demonstrated that synthetic analogs of lipid peroxidation products act through $K_v\beta2$ to alter potassium channel A-type inactivation in a substrate-specific manner. Lipid peroxidation products also prevent $K_v1.4$ inactivation, and $K_v\beta2$ shields $K_v1.4$ from this effect. $K_v\beta2$ cofactor exchange can be accelerated in a voltage-dependent manner to influence A-type inactivation, which has implications for $K_v\beta$ subunits in sleep-relevant neural circuits.

I have also discovered that Hyperkinetic is natively expressed in the dFB and that Hyperkinetic proteins engineered to accelerate cofactor exchange only partially rescue the sleep deficit of homozygous Hyperkinetic mutants, consistent with the idea that sensing, not catalysis, is the primary biological role of $K_v\beta$ subunits. Taken together, the data presented here provide evidence supporting the idea that $K_v\beta$ subunits act as voltage-sensitive enzymatic integrators of lipid peroxidation products to help influence sleep through modulating A-type currents.

Introduction

Neural and molecular mechanisms of sleep regulation in *Drosophila*

Despite decades of research into sleep and its ubiquity across the animal kingdom (Anafi et al., 2019), its biological purpose remains poorly understood. Better understanding its neuronal regulation may reveal insights about the nature of sleep's benefits and the consequences associated with impaired sleep (Joiner, 2016; Mignot, 2008). Two separate but interacting systems are thought to control sleep: circadian and homeostatic regulation (Borbély, 1982; Borbély, 2022; Ni et al., 2019).

The circadian system, which is based on cyclical external changes to which organisms must adapt, is well characterized (Allada et al., 2001; Crane and Young, 2014), and current research is actively investigating how circadian rhythms regulate sleep (Ni et al., 2019). The endogenous circadian clock underlying the circadian system drives cyclical patterns of protein expression to synchronize external 24-hour day-night cycles with animals' sleep-wake cycles (Allada et al., 2001; Dubowy & Sehgal, 2017).

In *Drosophila melanogaster*, a widely used model organism for studying circadian and homeostatic sleep regulation (Dubowy & Sehgal, 2017; Pimentel et al., 2016), circadian rhythms are driven by approximately 150 clock neurons in the brain, which are organized into distinct neuroanatomical clusters (Dubowy & Sehgal, 2017). Among these, the lateral neurons are critical for generating locomotor rhythms (Schlichting et al., 2019; Delventhal et al., 2019), and a diverse set of downstream circuits ultimately couple these rhythms to sleep regulation (Schwarz et al., 2021; Guo et al., 2016; Cavanaugh et al., 2014; Tabuchi et al., 2018). For instance, small ventrolateral neurons

(s-LNvs) connect to a dorsal group of clock neurons (DN1s) (Schwarz et al., 2021; King & Sehgal, 2020) that, through feedback onto other clock neurons, modulate onset and length of various aspects of *Drosophila* sleep architecture (Guo et al., 2016). DN1s also project to other brain regions involved in sleep-wake control (Artiushin & Sehgal, 2017) to couple clock neuron activity profiles to modulation of arousal circuits and consolidation of sleep (Cavanaugh et al., 2014; Tabuchi et al., 2018).

In contrast to the circadian system, much less is known about the neural mechanisms underlying the sleep homeostat, which monitors internal changes and then offsets accumulated sleep pressure by balancing wakefulness with sleep need, and how circadian and homeostatic circuits interact to influence sleep. As such, understanding which physiological and biochemical cues the sleep homeostat temporally integrates is expected to provide crucial clues to the function of sleep in the broader context of sleep regulation.

Previous work in *Drosophila* has identified a small cluster of 31 neurons innervating the dorsal fan-shaped body (dFB) of the central complex (Hulse et al., 2021) as a key region involved in homeostatic sleep regulation (Donlea et al., 2011; Donlea et a., 2014; Pimentel et al., 2016). The central complex, which has about 3,000 neurons (Hulse et al., 2021), is organized into several layers and integrates a wide array of sensory inputs (Wolff et al., 2015; Hulse et al. 2021) to influence an equally diverse set of downstream behaviors and functions, such as locomotion (Strauss 2002), memory (Sakai et al., 2012), social behaviors (Kacsoh et al., 2019), feeding (Sareen et al., 2021), nociception (Hu et al., 2018), courtship (Sakai & Kitamoto, 2006), vision processing (Weir & Dickinson, 2015), and sleep (Pimentel et al., 2016). Similarly, dFB

neurons within the central complex also receive a wide array of inputs from visual, mechanosensory (Hulse et al., 2021), and circadian cues (Schwarz et al., 2021, Ni et al., 2019), though much is still not know about how these upstream signals reach the dFB and how they interact with other inputs to converge on sleep phenotypes. Downstream outputs of the dFB are also poorly characterized, but it is known that dFB activity inhibits locomotor and visual activity in the context of sleep regulation (Donlea et al., 2018).

Interestingly, it is not known whether the dFB neurons can be treated as a functionally homogenous group of neurons. It has been found that different dFB neurons differentially express 5HT2b serotonin receptors to affect sleep (Qian et al., 2017), and ongoing, unpublished work is exploring the possibility of dFB functional heterogeneity in driving sleep. As such, future work based on a detailed connectome of the central complex (Hulse et al., 2021), will need to better elucidate the synaptic connections and signaling pathways that converge on dFB neurons and the downstream behavioral outputs that are shaped by dFB activity based on potential heterogeneity among the dFB population. Further transcriptomic and proteomic, electrophysiological, and behavioral experiments targeting better defined subsets of dFB neurons will also be needed to better understand the precise nature of how the dFB influences sleep.

Although much is still unknown about individual dFB neurons and their functional connectivity, on the entire dFB population level, previous work has shown that dFB neurons induce sleep when activated and lead to insomnia when activity is compromised, thereby implicating them as the sleep homeostat’s output arm (Donlea et

al., 2011; Donlea et al., 2014). Further work has uncovered the biophysical properties of dFB neurons that allow the dFB to function as a homeostatic sleep-regulating switch through its electrical excitability (Donlea et al., 2014; Pimentel et al., 2016). When sleep need accumulates, such as in sleep-deprived flies, dFB neurons increase their electrical excitability (ON state) to drive sleep (Donlea et al., 2014). Conversely, dFB activity decreases in well-rested flies and the dFB neurons are in an OFF state, reflected in electrical silence, when the fly is awake (Donlea et al., 2014; Pimentel et al., 2016). Changes in sleep pressure are thus represented in the corresponding electrical excitability of dFB neurons (ON-OFF switch) through which self-correcting feedback generates cycles of sleep and wakefulness (Figure 1) (Donlea et al., 2018; Pimentel et al., 2016).

Inherent to the regulation of dFB neurons' excitability is the regulation of their ion channels. Dopamine—a wake-promoting neurotransmitter in *Drosophila* (Ueno et al., 2012)—binding to Dop1R2 receptors, a GPCR, on dFB neurons initiates awakening by causing transient hyperpolarization and a longer lasting suppression of excitability, thus allowing for both quick and sustained responses to arousing events (Pimentel et al., 2016). The sustained activity suppression is mediated by altered regulation of two potassium channels: A-type currents carried through Shaker, a voltage-gated potassium ion channel (K_v), are downregulated, whereas voltage-independent leak currents carried through Sandman, a newly identified two-pore domain channel (K2P), are upregulated as dopamine causes translocation of Sandman to the plasma membrane (Pimentel et al., 2016). These two molecular events in conjunction silence dFB neurons (ON-OFF transitions) to allow the fly to stay awake.

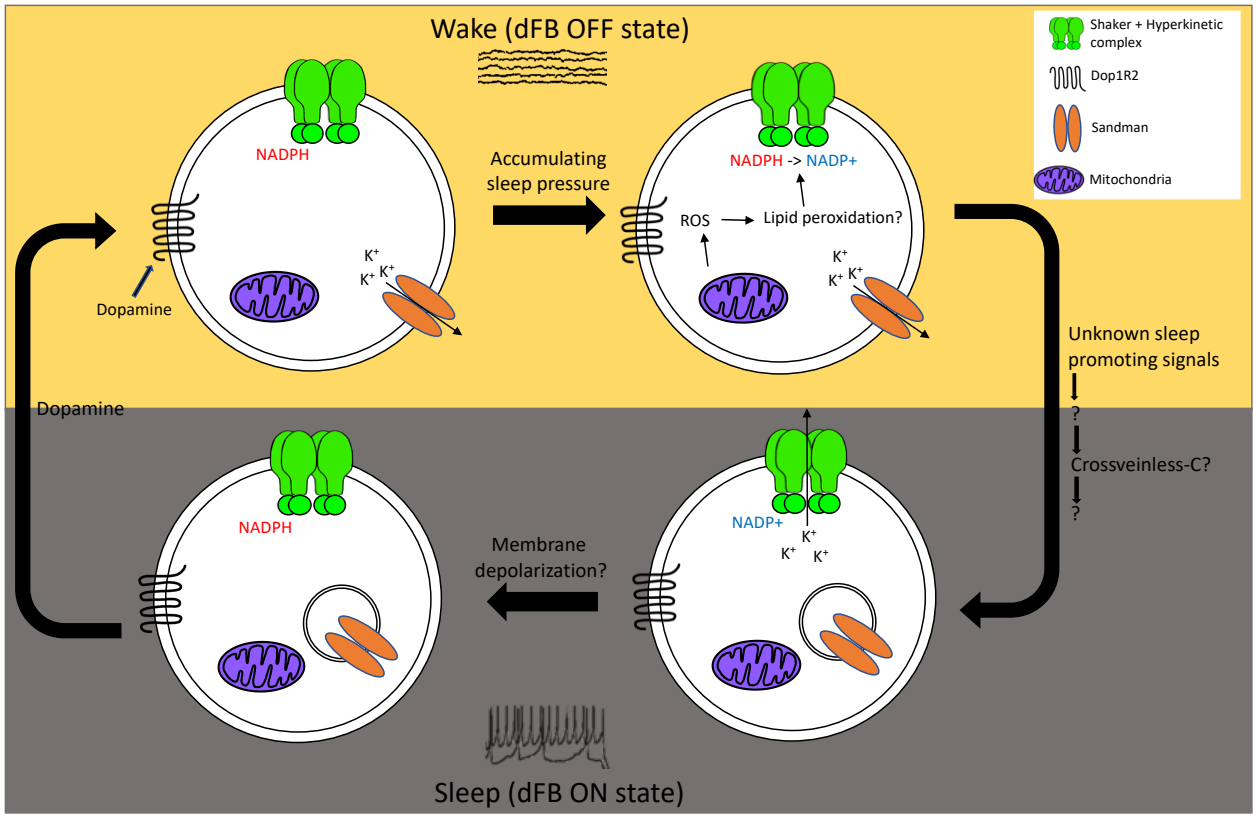


Figure 1. Model of homeostatic sleep regulation in *Drosophila* in the dFB. (Top) To initiate waking, dopamine binds to Dop1R2, a GPCR, receptors on the dFB, which leads to downregulation of Shaker, a K_V channel with a T1 domain, currents and leads to insertion of Sandman, a K2P channel, in the plasma membrane. Potassium leak currents through Sandman then predominate and lead to electrical silence within the dFB while the fly is awake. When sleep pressure accumulates throughout the day, mitochondrial ROS production accumulates and leads to oxidation of NADPH to NADP+, thereby allowing the oxidation state of Hyperkinetic's cofactors to act as biochemical memory and couple sleep pressure to electrical excitability. However, Shaker currents cannot help drive the fly to sleep since Sandman leak currents still prevail. (Bottom) When currently unknown sleep promoting signals arrive, they lead to the internalization of Sandman, thereby allowing dFB neurons to fire and delayed Shaker currents to prolong spiking. Near the end of the night, NADPH cofactors replace NADP+, and the cycle repeats itself when awakening dopaminergic signals arrive. Schematic adapted from Lyons & Rihel (2020) and Xu et al., (2019).

Conversely, understanding what mediates the transition to switching dFB neurons into their electrically active state (OFF-ON transitions) to drive sleep would reveal insight into how sleep debt and waking time are neurally encoded. The relevant signals must influence Sandman internalization and Shaker current modulation

(Pimentel et al., 2016). Ongoing work suggests that Crossveinless-C, a Rho-GTPase, is potentially involved in Sandman internalization (Donlea et al., 2014), though complete details are lacking about what potential sleep-inducing signals converge on the dFB. Recent work has focused on the roles that Shaker and its auxiliary beta subunit Hyperkinetic have in increasing dFB neuronal excitability and influencing sleep through Hyperkinetic's redox sensing (Kempf et al., 2019). When sleep pressure accumulates and dFB neurons are in their OFF state, an increase in mitochondrial reactive oxygen species (ROS) generation alters the redox state of dFB neurons (reviewed in more detail later in the introduction) (Kempf et al., 2019). This increase is stored as biochemical memory of sleep pressure through oxidative conversion of Hyperkinetic's NADPH cofactor to NADP+, which increases dFB action potential generation by delaying Shaker inactivation (Kempf et al., 2019).

From these studies, it is known that dopamine drives the dFB ON-OFF transition in which Sandman insertion into the plasma membrane leads to potassium leak currents silencing dFB neurons during the OFF state (Pimentel et al., 2016). Shaker currents are also downregulated in the OFF state (Pimentel et al., 2016), presumably due to Hyperkinetic's replacement of its bound NADP+ cofactors with NADPH during the ON-OFF transition. Then, throughout the OFF state while dFB neurons are silent, ROS accumulation would lead to NADP+ being predominantly bound to Hyperkinetic, and when the relevant sleep signals arrive to internalize Sandman, delayed inactivation of Shaker currents due to Hyperkinetic's NADP+ cofactors drive the OFF-ON transition to cause sleep by increasing dFB electrical activity (Kempf et al., 2019). While dFB neurons are in the ON state, Hyerpkinetic's redox memory of accumulated sleep

pressure should dissipate through currently unknown mechanisms, and this cycle would then repeat itself again when dopaminergic signaling arrives to initiate awakening (Ueno et al., 2014; Pimentel et al., 2016). This model suggests that dFB neurons may endogenously contain all the necessary components to function as a homeostatic sleep switch to drive sleep when active (Figure 1) (Donlea et al., 2014; Pimentel et al., 2016; Donlea at el., 2018; Kempf et al. 2019), though other neural circuits act through the dFB to also influence sleep.

Although much is unknown about dFB functional connectivity, previous work has identified another component of the sleep homeostat in *Drosophila*: R5 neurons in the ellipsoid body, also contained within the central complex (Liu et al., 2016). R5 neurons encode sleep drive, and though there is no direct connectivity between dFB and R5 neurons, they communicate indirectly through recurrent circuitry (Donlea et al., 2018). R5 neurons increase their activity following prolonged wakefulness, such as with sleep deprivation (Liu et al., 2016). Following sleep deprivation, R5 neurons drive rebound sleep through dFB neuron activation to offset accumulated sleep pressure (Liu et al., 2016; Donlea et al., 2018), thereby implicating R5 neurons as a homeostatic sleep integrator through its ability to encode sleep pressure.

dFB neurons indirectly inhibit R5 neurons by inhibiting intermediary Helicon cells, which then activate R5 neurons (Donlea et al., 2018). Helicon cells drive locomotor activity coupled to visual systems in the context of sleep (Donlea et al., 2018). Thus, during sleep when dFB neurons are active, they attenuate sensory inputs and locomotor activity by inhibiting Helicon cells and dissipate accumulated sleep pressure in R5 neurons through indirectly inhibiting them through Helicon cells (Donlea et al., 2018).

Conversely, when flies are sleep deprived and R5 neurons store sleep pressure to become active, they indirectly activate dFB neurons to drive rebound sleep (Liu et al., 2016; Donlea et al., 2018). In this manner, sleep deprivation leads to increased activity in R5 neurons, which then communicate this sleep need to dFB neurons. dFB neurons in turn cause sleep and inhibit R5 activity through Helicon cells, thereby completing this recurrent circuit to offset sleep deprivation (Figure 2).

Interestingly, though much is unknown about how the circadian and homeostatic systems interact, in part due to an incomplete understanding of the neural and molecular mechanisms of homeostatic sleep regulation, recent work has uncovered potential mechanisms through which R5 and dFB neurons intersect with circadian signals to influence sleep (Figure 2) (Ni et al., 2019; Schwarz et al., 2021; Guo et al., 2018; Lamaze et al., 2018). Circadian s-LNvs connecting to DN1s (Schwarz et al., 2021), specifically Anterior-Projecting Dorsal Neurons, have both inhibitory and excitatory connections to tubercular bulbar neurons that function upstream of ellipsoid body neurons (Guo et al., 2018; Lamaze et al., 2018). These tubercular bulbar neurons in turn have both indirect and direct connections with R5 neurons and have been shown to play a role in sleep regulation (Guo et al., 2018; Lamaze et al., 2018). Similarly, a subset of circadian pacemaker neurons has been shown to directly synapse with dFB neurons to regulate sleep, providing a direct connection between circadian and homeostatic centers (Ni et al., 2019). Further work has uncovered a subset of *hugin*$^{+}$ neurons that integrate signals from dFB neurons and from circadian inputs to modulate downstream circadian inputs and ultimately regulate sleep (Schwarz et al., 2021). Future work in this field will continue to elucidate neural and molecular mechanisms by

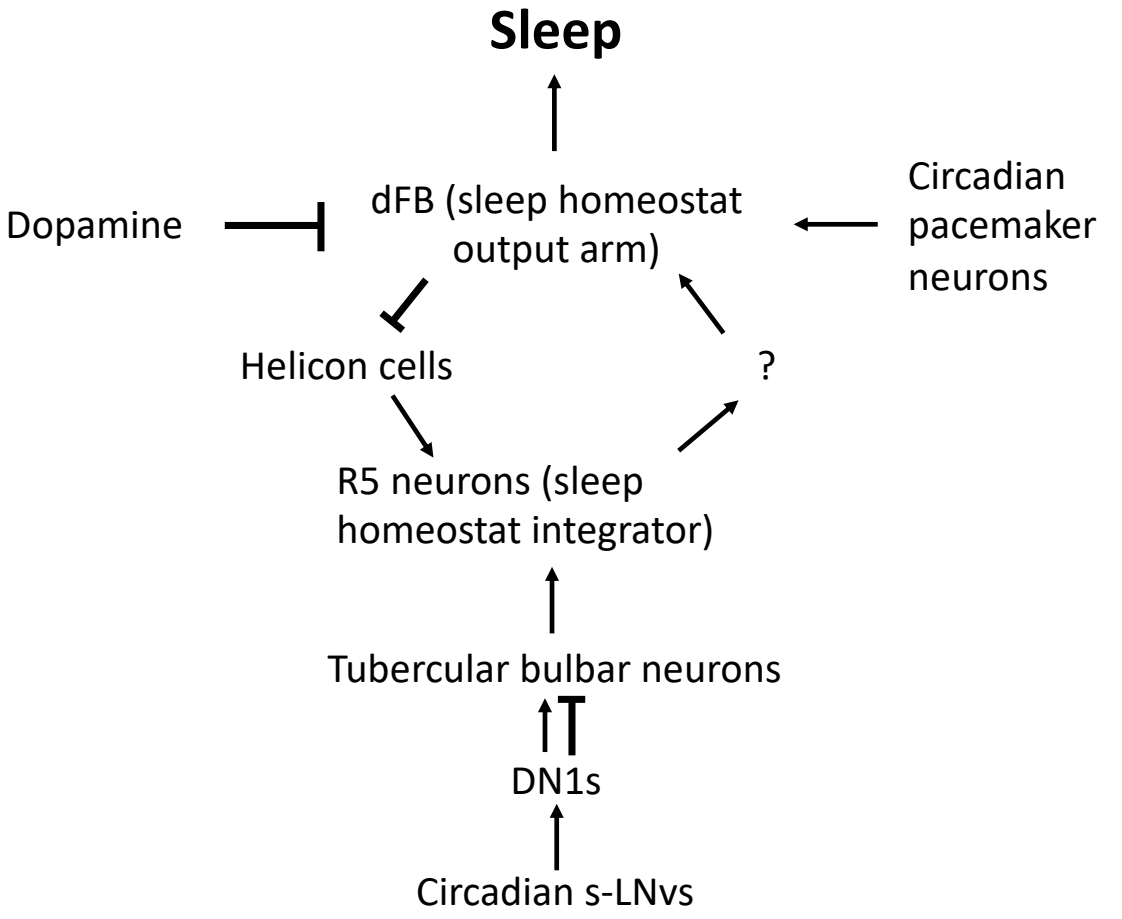


Figure 2. Intersecting circadian and homeostatic circuits contribute to sleep regulation. Although much is unknown about how the sleep homeostat works and how circadian and homeostatic sleep signals work either together or independently to regulate sleep, several components of such a system are known. Recurrent circuitry links the dFB, the sleep homeostat's output arm, to R5 neurons, the sleep homeostat integrator of sleep pressure. Within this recurrent circuit, neural pathways can receive input form circadian systems to jointly influence sleep. Adapted from Lyons & Rihel (2020).

which circadian and homeostatic signals intersect, particularly as more about the homeostatic system is uncovered.

In the context of homeostatic sleep regulation in *Drosophila*, this thesis has focused on further characterizing the molecular aspects of redox regulation of Hyperkinetic and A-type potassium currents.

K_v subunits and their role in sleep regulation

Shaker and Hyperkinetic, a *Drosophila* $K_v\beta$ subunit, bind at the plasma membrane to form an ion channel complex (Chouinard et al., 1995). Similarly, the mammalian homologs from the Shaker voltage-gated potassium channel family ($K_v\alpha$) and their beta subunits ($K_v\beta$) co-assemble as tetrameric ion channel complexes (Long et al., 2005; Gulbis et al., 1999; Gulbis et al., 2000). Shaker and Hyperkinetic mutant flies have reduced sleep (Cirelli et al., 2005; Bushey et al., 2007), and similar findings have been demonstrated in mice with corresponding $K_v\alpha$ mutants (Douglad et al., 2007; McCormack et al., 2002), highlighting the importance of K_v subunits in sleep regulation.

The Shaker voltage-gated potassium channel family (K_v1), named based on their similarity to Shaker, is a group of transmembrane potassium ion channels that broadly regulate membrane potential and excitability (Jan & Jan, 2012) in a wide range of physiological contexts across the nervous, cardiovascular, endocrine, and immune systems (Raph et al., 2019). There are 12 subfamilies of mammalian K_v ion channels (Gonzalez et al., 2012), and work in this thesis has focused on several K_v1 channels due to Shaker's role in sleep regulation (Pimentel et al., 2016; Kempf et al., 2019). K_v1 channels are composed of tetrameric, transmembrane assemblies that are highly selective for potassium ions (Long et al., 2005; Doyle et al., 1998). Two primary types of these K_v channels have been characterized: rapidly inactivating (A-type) channels and delayed rectifiers channels that demonstrate much slower inactivation (Pongs et al., 1999). However, K_v1 channels natively form heterotetrametric complexes with each other, which leads to variable electrophysiological properties and increased diversity of channel and current profiles (Scott et al., 1994; Coetzee et al., 1999). Assembly with

$K_v\beta$ subunits further increases channel diversity through altered inactivation kinetics and the possibility of conferring A-type inactivation on delayed rectifier channels (Pongs et al., 1999).

As such, $K_v\beta$ subunits play a unique role in K_v channel kinetics. $K_v\beta$ subunits belong to the aldo-keto reductase superfamily, a group of oxidoreductase enzymes that reduce carbonyl compounds (Gulbis et al., 1999). Aldo-keto reductases, including $K_v\beta$ subunits, are highly conserved enzymes across the animal kingdom and have significant structural similarity: TIM barrel structures house C-terminal active sites that catalyze compound reduction in a cofactor dependent fashion (Hoog et al., 1994; Barski et al., 2008). However, unlike other soluble aldo-keto reductases found in the cytoplasm, $K_v\beta$ subunits are bound to $K_v\alpha$ subunits at the plasma membrane (Long et al., 2005). The N-terminal domains of the $K_v\alpha$ tetrameric subunit complex form a docking platform, through which $K_v\beta$ subunits can bind to $K_v\alpha$ T1 domains to inactivate the ion channel (Long et al., 2005; Gulbis et al., 2000).

As confirmation of their enzymatic properties, $K_v\beta$ subunits are structurally similar to aldo-keto reductases (McCormack & McCormack, 1994; Gulbis et al., 1999; Chouinard et al., 1995), bind NADPH cofactors in their active site near the substrate binding site (Gulbis et al., 1999), and can alter $K_v\alpha$ voltage-dependent inactivation kinetics by reducing aldehyde-containing molecules and oxidizing NADPH (Rettig et al., 1994; Weng et al., 2006; Tipparaju et al., 2008). In addition to modulating $K_v\alpha$ channel kinetics, $K_v\beta$ subunits have also been shown to form dynamic complexes with $K_v\alpha$ subunits (Shi et al., 1996). These subunits co-assemble in the endoplasmic reticulum early in biosynthesis (Shi et al., 1996; Nagaya & Papazian, 1997), and $K_v\beta$ subunits

may have a chaperone role in boosting channel expression at the surface (Shi et al., 1996) and regulating targeting of the channels to specific neuronal areas (Campomanes et al., 2002).

In the context of sleep, one functional reason for linking a neuron's excitability to its biochemistry through $K_v\beta$ subunits implicates Hyperkinetic, which has significant sequence homology with mammalian $K_v\beta$ subunits (see Results Chapter 3 for structural diagrams), as a mediator between oxidative stress and sleep (Kempf et al., 2019). As aldo-keto reductases, $K_v\beta$ subunits may be able to couple their redox catalytic capabilities to altered channel kinetics to reflect changes in cellular redox states (Long et al., 2005; Kempf et al., 2019). Indeed, sleep loss in *Drosophila* has been shown to elevate levels of mitochondrially generated ROS that slow A-type current inactivation and increase action potential frequency in dFB neurons (Kempf et al., 2019). Critically, this process is dependent upon Hyperkinetic's oxidoreductase activity, suggesting that Hyperkinetic's redox sensing ability could influence how sleep deficits are monitored and dissipated through its effects on Shaker (Kempf et al., 2019). Since $K_v\beta$ subunits tightly bind NADPH (Gulbis et al., 1999) and have slow cofactor exchange rates (Weng et al., 2006), increased ROS production stemming from prolonged wakefulness may alter the ratio of Hyperkinetic's bound NADPH to NADP+ to act as biochemical sleep memory (Kempf et al., 2019). As a result, Hyperkinetic acts as a temporal and biochemical integrator of ROS during waking through its ability to convert NADPH to NADP+ and hold on to the oxidized cofactor as a biochemical memory of accumulated sleep pressure. Coupling between the active site of the $K_v\beta$ subunit and the inactivation

gate of the channel could link the stored NADPH to NADP+ ratio to the induction of sleep (Figure 1).

These results help explain why earlier studies observed that Shaker and Hyperkinetic mutants had insomniac phenotypes (Cirelli et al., 2005; Bushey et al., 2007), though the biophysical properties underling these mutant phenotypes remain unknown. Without functional Shaker channels in the dFB, flies would presumably not be able to repolarize their membranes as quickly following actional potentials in the dFB ON state, thereby leading to less neuronal activity at night and thus less sleep (Pimentel et al., 2016; Kempf et al., 2019). Similarly, for Hyperkinetic mutants, accumulated ROS signals presumably would not be able to delay Shaker inactivation to repolarize membrane potentials as quickly, thereby also leading to reduced sleep.

Taken together, these findings about Hyperkinetic's catalytic role in sleep regulation raise the possibility that sleep profiles can be altered through $K_v\beta$ subunit substrates, which could influence targeted drug discovery, and catalysis. These findings lay the foundation for my thesis work, which is subdivided into three distinct chapters and aims presented below.

$K_v\beta$ subunit substrates and catalysis in sleep regulation

Chapter 1: Mass spectrometry (MS) characterization of $K_v\beta2$ native ligands

It is still unknown what endogenous substrates bind to $K_v\beta$ subunits. An unresolved electron density overlying the hydrophobic $K_v\beta2$ active site of a purified $K_v1.2$-$K_v\beta2$ complex (Figure 3) suggests that a heterogeneous mix of native ligands binds to $K_v\beta$ subunits and leads to the oxidation of NADPH (Long et al., 2005). Potential

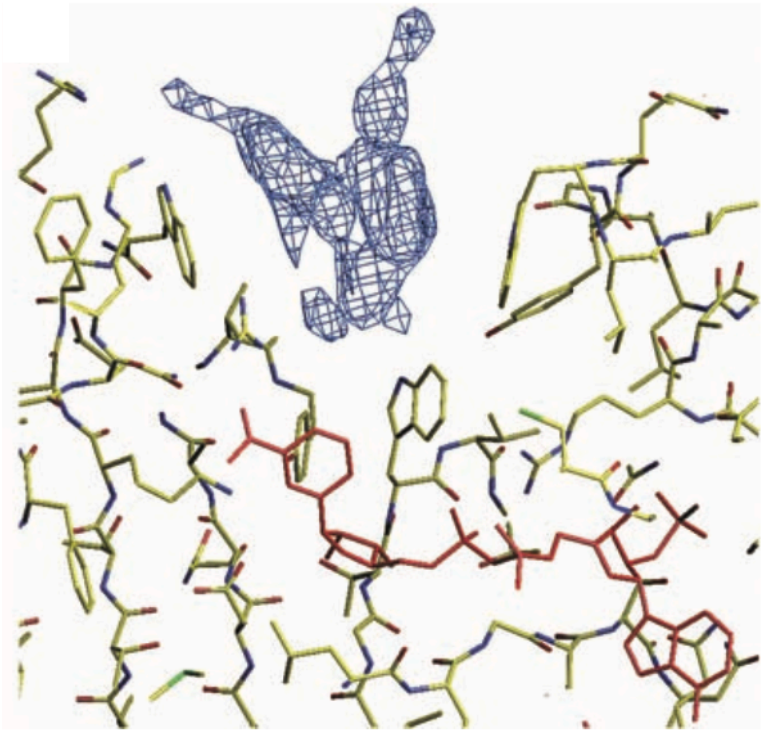


Figure 3. An unresolved electron density overlying the $K_v\beta2$ active site. Figure taken from Long et al. (2005), who resolved the structure of the $K_v1.2$-$K_v\beta2$ complex. They found an unresolved electron density in the active site of $K_v\beta2$, which could represent endogenous substrates. The chemical identity of this unresolved electron density, however, remains unknown.

insight into the endogenous substrates of $K_v\beta$ subunits comes from the observation that increased ROS production from the mitochondria led to oxidation of Hyperkinetic's NADPH cofactor (Kempf et al. 2019).

ROS, a broad term encompassing a wide array of oxygen derivatives produced from aerobic metabolism, are unstable and short-lived (Sies & Jones, 2020). A major source of endogenous ROS production comes from the mitochondrial electron transport chain (Murphy, 2009; Wong et al., 2019). Indeed, it has been shown that mitochondrial ROS production was elevated in the dFB following sleep deprivation (Kempf et al., 2019). When sleep need accumulates as dFB neurons are in the OFF state, low metabolic demands in the dFB may lead to an accumulation of ATP that causes

electrons to leak from the mitochondrial transport chain and transfer to oxygen, thereby producing ROS (Balaban et al., 2005; Murphy, 2009; Parvez et al., 2018). Since ROS are short-lived and since the mitochondria is spatially separated from the plasma membrane where Hyperkinetic acts, secondary signaling molecules to convey the redox relay are needed (Sies & Jones, 2020). One possibility concerns lipid peroxidation, whereby oxidized polyunsaturated fatty acids generate lipid hydroperoxides and downstream radicals to perpetuate redox signaling (Higdon et al., 2012). Lipid peroxidation products as secondary messengers of redox signaling are critical for signaling within the immune system and particularly with regards to inflammation (Czapski et al., 2016) and thus could potentially endogenously react with $K_v\beta$ subunits to regulate sleep.

As such, since ROS species are short-lived, they may react with nearby phospholipids to produce more stable lipid peroxidation products with aldehyde and ketone functional groups suitable for aldo-keto reductases that can diffuse to the plasma membrane and react with $K_v\beta$ subunits (Gulbis et al., 1999; Parvez et al., 2018; Esterbauer et al., 1991). Indeed, it has been shown that $K_v\beta2$ can reduce the byproducts of lipid oxidation *in vitro* (Tipparaju et al., 2008; Xie et al., 2011). Therefore, the first part of my thesis seeks to uncover the identity of $K_v\beta$ subunit native ligands and examines whether lipid peroxidation products natively bind to $K_v\beta$ subunits.

Chapter 2: $K_v\beta2$'s influence on A-type current inactivation

The second part of my thesis tests whether lipid peroxidation products can influence A-type inactivation through $K_v\beta$ subunits. Previous work has demonstrated

that small-molecule substrates containing an aldehyde group can modulate the inactivation of K_v1.4's characteristic A-type currents, which are similar to Shaker's A-type currents, through $K_v\beta$2 (Weng et al., 2006), and it is known that Hyperkinetic's redox sensing capabilities coupled to delayed A-type inactivation plays a role in sleep (Kempf et al., 2019). However, lipid peroxidation products as potential $K_v\beta$ subunit substrates for A-type current modulation have not been directly tested, which this chapter will address.

This section will also examine whether lipid peroxidation products can influence $K_v\alpha$ subunit inactivation in the absence of $K_v\beta$ subunits. Previous work has shown that inside-out patches, which expose the membrane to air to cause oxidation, of K_v1.4 prevents the complete inactivation of the ion channel (Ruppersberg et al., 1991). It was found that this effect was caused by cysteine oxidation on the 13th residue of K_v1.4's N-terminal inactivation chain since a C13S mutation abolished this effect (Ruppersberg et al., 1991). However, this effect has not been replicated with aldehyde- and ketone-containing molecules in patch clamp recordings of K_v1.4, so it is unknown if this phenomenon can be replicated through biological substrates. Validation of this phenomenon would also be important to properly study how lipid peroxidation products influence A-type inactivation through $K_v\beta$ subunits since the ion channel needs to be controlled for. If lipid peroxidation products can influence $K_v\alpha$ subunit inactivation, then perhaps $K_v\beta$ subunits can protect $K_v\alpha$ subunits from the effects of oxidative stress (Pérez et al., 2008; Raph et al., 2019).

The second part of my project will also test whether $K_v\beta$ subunit cofactor exchange can be accelerated through voltage changes in the context of its capacity as

biochemical memory storage (Gulbis et al., 1999; Pan et al., 2008a). If Hyperkinetic's pool of NADPH cofactors gradually becomes oxidized to NADP+ during wake to regulate sleep through modulating Shaker currents, the NADPH:NADP+ ratio should reset during sleep so the cycle can repeat upon waking. If $K_v\beta$ subunit enzymatic activity were gated by voltage, NADP+ release would be impaired during waking because the dFB neurons are electrically silent, but during sleep when the voltage threshold for K_v ion channels is surpassed as dFB neurons fire action potentials, NADP+ would be released (Figure 1). NADPH should then replace NADP+ since there is a higher concentration of cytoplasmic NADPH and since $K_v\beta$ subunits have a higher binding affinity for NADPH than for NADP+ (Liu et al., 2001). Through this, accumulated sleep pressure and its dissipation would be encoded by the biophysical properties and biochemical state of K_v ion channels and their $K_v\beta$ subunits.

Chapter 3: Altering sleep profiles through manipulating Hyperkinetic's cofactor exchange rate

The importance of Hyperkinetic's catalytic capabilities in sleep regulation further raises the possibility that sleep profiles can be altered by manipulating the catalytic efficiency of $K_v\beta$ subunits. Expressing wild-type Hyperkinetic in the dFB in a Hyperkinetic null background rescues the insomniac phenotype that a Hyperkinetic null background induces, but expressing a catalytically dead Hyperkinetic mutant in the dFB fails to correct the insomnia (Kempf et al., 2019). Aside from a catalytically dead Hyperkinetic mutant, no other mutants have been tested.

Since $K_v\beta$ subunits have higher binding affinity for NADPH over NADP+ (Liu et al., 2001) and since the cofactor exchange rate is the rate-limiting step in $K_v\beta$ subunit enzymatic reactions (Weng et al., 2006), it may be possible to directly manipulate sleep profiles by altering $K_v\beta$ subunits' cofactor exchange rate. If $K_v\beta$ mutants have a higher cofactor exchange rate, then their ability to integrate ROS signals over time will be compromised, leading to sleep loss. The third part of my project tests this idea by designing Hyperkinetic mutants whose cofactor exchange rates are predicted to be elevated, confirming this prediction *in vitro*, and measuring the effects of these mutations on sleep after expressing them in the dFB in a Hyperkinetic null background. To ensure correct folding, assembly, and trafficking of the engineered proteins, future work will test the homologous $K_v\beta$ mutations in the HEK-293 expression system for their ability to confer inactivation on $K_v1.4$.

Taken as a whole, my projects will test whether $K_v\beta$ subunits can act as voltage-sensitive enzymatic integrators of lipid peroxidation products to help influence sleep through modulating A-type currents.

Methods

Cell culture

Frozen HEK-293 cells were stored in liquid nitrogen in cryotubes containing a fetal bovine serum solution with 10% DMSO. Adherent HEK-293 cells were grown in monolayer cell culture flasks in DMEM supplemented with penicillin-streptomycin and 10% fetal bovine serum at 37 °C and 5% CO_2. Cells were passaged via trypsinization every 48 hours. Cells were pelleted by centrifuging at 1000 RPM for 5 minutes and resuspended in fresh media.

Plasmids and mutagenesis

Mutagenesis experiments were performed using NEB's Q5 Site-Directed Mutagenesis Kit, which employs non-overlap PCR that uses primers containing the desired mutations to amplify the entire plasmid. Primer design was done using NEB's NEBaseChanger, which also provides the ideal annealing temperature for PCR. Plasmids were amplified in and purified from One Shot TOP10 chemically competent *E. coli*. Bacteria were stored at -80 °C and thawed on ice. Once thawed, plasmid DNA was added and the bacteria were heat shocked at 42 °C. S.O.C. media was added and the bacteria were placed in a shaking incubator at 37 °C and 225 RPM for 1 hour. Bacteria were then grown on standard LB agar plates with the appropriate antibiotic (50 ug/ml of ampicillin or kanamycin) overnight at 37 °C. Single colonies were picked for amplification in LB broth containing the appropriate antibiotic overnight at 37 °C and 225 RPM. Plasmids

were then purified using Macherey Nagel's silica membrane NucleoSpin plasmid columns. All constructs were validated via Sanger sequencing.

Transfection and stable cell line generation

HEK-293 cells were transfected using Lipofectamine 3000. To create a stable cell line, cells were transfected with a plasmid containing a CMV promoter region expressing a C-terminally FLAG-tagged mouse $K_v\beta2$ construct with a downstream internal ribosome entry site (IRES) sequence with puromycin resistance. 48 hours post-transfection, cells were passaged into fresh media containing puromycin (2 ug/ml) to select for puromycin resistant cells. Selected cells were continually passaged in media containing puromycin. To avoid protein aggregation, the first 35 N-terminal amino acids of $K_v\beta2$ were removed, thereby leaving amino acid residues 36-367 (LQFYR…KDYRS) (Gulbis et al., 1999). A linker peptide sequence of TRTRPLEQKLISEEDLAANDIL connects $K_v\beta2$ with the C-terminal FLAG tag, giving a total theoretical monomeric mass of 40,910.05 Da for the entire $K_v\beta2$-FLAG construct.

Immunofluorescence imaging

HEK-293 cells were grown on glass microscope coverslips. They were then washed with PBS for 5 minutes, fixed in 4% paraformaldehyde in PBS for 15 minutes, washed three times with PBS for 5 minutes per wash, permeabilized with 0.1% Triton X-100 in PBS for 15 minutes, washed with 0.06% Tween-20 in PBS for 5 minutes, washed twice with PBS for 5 minutes, and blocked for one hour at room temperature in 10% normal goat serum in PBS. Primary antibodies were diluted in 10% normal goat serum in PBS

and incubated with the cells overnight at 4 °C. Cells were then washed three times with PBS for 5 minutes, incubated with fluorescent secondary antibodies diluted in 10% normal goat serum in PBS for 1 hour shielded from light, stained with Hoescht diluted in PBS, and washed three times with PBS for 5 minutes at room temperature before being mounted on a microscope slide with VECTASHIELD Antifade Mounting Medium. Coverslips were then imaged using a Leica confocal laser scanning microscope and images were processed on ImageJ.

Purification of FLAG-tagged proteins

HEK-293 cells expressing FLAG-tagged constructs were scraped with ice-cold PBS and centrifuged at 1000 RPM for 5 minutes at 4 °C. All remaining steps were performed at 4 °C and on ice. Cell pellets were then resuspended in a 50 mM Tris HCl, pH 7.5, 150 mM KCl buffer containing protease inhibitors. For the extraction of membrane proteins, the detergent *n*-dodecyl-β-D-maltopyranoside (DDM) was used. To extract soluble proteins, no exogenous lipids or detergents were used. Cells were lysed with a sonication probe using 60% amplitude with 10 seconds on and 20 seconds off for 30 minutes and then centrifuged at 20,000 *g* for 20 minutes. To remove contaminants, the collected supernatant was pre-cleared via incubation with mouse IgG for 2 hours on a roller and then centrifuged. The harvested supernatant was then incubated with anti-FLAG magnetic beads on a roller for 3 hours. The beads were washed five times 30 minutes each on a roller with the lysis buffer. Protein was then eluted with 0.05 mg/ml 1x FLAG peptide in lysis buffer with 10% glycerol for 40 minutes on a roller. Eluted protein was then concentrated as needed.

Mass spectrometry

All MS experiments were performed by collaborators in the Robinson group with experimental guidance and input from me.

POVPC reduction and binding

The following protocol was optimized and performed by collaborators in the Robinson group. To test $K_v\beta2$ activity with POVPC, $K_v\beta2$ was buffer exchanged into 200 mM ammonium acetate and a 17 mM POVPC stock solution in water was made. Further dilutions were done as necessary to achieve the proper concentrations. For reduction studies, 40 uM of $K_v\beta2$ was incubated with 40 uM of POVPC at a 1:1 ratio. The mixture was incubated at 37 °C for 3 hours. The samples were then boiled at 95 °C for 30 minutes and centrifuged at 20,000 g for 20 minutes to release the substrates. The supernatant was harvested for MS analysis on Eclipse (Thermo Fisher). For binding studies, 40 uM of $K_v\beta2$ was incubated with either 40 uM or 2.8 mM POVPC at a 1:1 ratio at either 4 or 37 °C for 5 minutes. The incubation time for binding experiments was shorter than reduction experiments to try to capture the binding that precedes catalysis on native MS.

Western blot and Coomassie staining

Protein samples were boiled at 95 °C for 5 minutes in Laemmli buffer and β-mercaptoethanol and run in pre-cast 4-12% Bis-Tris protein gels. For *Drosophila*, fly heads were homogenized before being boiled. InstantBlue staining was used for

Coomassie visualization. For Western blots, following protein transfer to a PVDF membrane, membranes were blocked in 5% milk in TBST (0.1% Tween-20 in tris-buffered saline) for 1 hour at room temperature and incubated with primary antibodies diluted in 5% milk in TBST overnight at 4 °C. Membranes were then washed three times for 5 minutes each with TBST, incubated with HRP conjugated secondary antibodies diluted in 5% milk in TBST for 1 hour, washed three times for 5 minutes each with TBST at room temperature, and imaged using enhanced chemiluminescence.

Electrophysiology

Transiently transfected HEK-293 cells were trypsinized and plated on glass coverslips pre-coated with poly-L-lysine. The extracellular solution, pH 7.4, consisted of 5 mM KCl, 140 mM NaCl, 10 mM HEPES, 10 mM glucose, 1 mM $MgCl_2$, and 2 mM $CaCl_2$. A GFP microscope was used to select transfected cells containing constructs of interest co-expressed with a downstream IRES-EGFP. Patch pipettes pulled from borosilicate glass capillaries to a resistance of 2-3 MΩ were filled with an internal solution, pH 7.3, consisting of 80 mM potassium aspartate, 60 mM KCl, 10 mM HEPES, 10 mM glucose, 5 mM EGTA, 1 mM $MgCl_2$, and 2 mM MgATP. Various substrates of interest were diluted into the intracellular or extracellular solution as needed at the concentrations (100 uM 4-ONE, 100 uM 4-HNE, 100 uM PGD_2, and 12 mM methylglyoxal) used in the previous biochemical studies of $K_V\beta2$ *in vitro* (Tipparaju et al., 2008). Cells were monitored during recordings to ensure substrate concentrations did not affect viability. Similar concentrations of substrates have been used by other lab members successfully. Voltage clamp recordings of single cells started at a holding potential of -

80 mV and were stepped from -100 mV to 50 mV using 10 mV steps (1 second duration). For the depolarization protocol, the holding potential was changed from -60 mV to 10 mV at 10 Hz (3 ms duration) for 10 minutes. Background subtracted currents were analyzed in Igor. A double exponential function was fitted to each curve to calculate inactivation time constants.

Drosophila melanogaster culture and constructs

Flies were reared at 25 °C on a 12 hour light:12 hour dark cycle. They were grown on standard brown food (the following reagents were added to 32 L of water: 216 g of agar, 800 g of yeast, 2000 g of cornmeal, 1.2 L of molasses, 134.4 mL of acid mix, 44.8 g of tegosept, and 224 mL of ethanol). The driver line *R23E10-GAL4* was used to target dFB neurons. Hyperkinetic sequences were subcloned into a pJFRC-MUH plasmid containing 10x UAS promoter sequences and injected into larvae on the second chromosome through BestGene. UAS-Hyperkinetic constructs were then crossed into a homozygous Hyperkinetic null (Hk^1) background.

Fly brain dissections and staining

Male flies were anesthetized on ice and dissected in PBS. Brains were fixed in 4% paraformaldehyde in PBS for 20 minutes and then washed three times with PBST (0.5% Triton X-100 in PBS) for 20 minutes each at room temperature. Brains were blocked in 10% normal goat serum in PBST overnight at 4 °C and then incubated with primary antibodies diluted in 10% normal goat serum in PBST for 48 hours at 4 °C. Brains were washed four times with PBST for 30 minutes each at room temperature, incubated with

secondary antibodies diluted in 10% normal goat serum in PBST for 24 hours at 4 °C, and washed four times with PBST for 30 minutes each at room temperature before being mounted on a microscope slide with VECTASHIELD. The slides were then imaged on a Leica confocal laser scanning microscope and images were processed using ImageJ.

Sleep experiments

Mated female flies 3-days post eclosion were loaded into individual 65 mm glass tubes and placed in Trikinetics *Drosophila* Activity Monitor systems that use infrared beam breaks to track activity. Flies were housed at 25 °C under 12 hour light:12 hour dark cycles. Periods of inactivity longer than 5 minutes were considered sleep. Data were analyzed in MATLAB and sleep profiles from days 2-3 were averaged.

CRISPR knock-in *Drosophila melanogaster*

Flies with an N-terminal FLAG tag for Hyperkinetic isoforms RE, RK, RL, and RM were created using CRISPR knock-in through WellGenetics in a w1118 background. CRISPR-Cas9 genome editing of the genomic Hk site was accomplished through homology-dependent repair using one guide RNA and a plasmid donor. The FLAG construct was inserted after the first methionine, and sequences encoding a 4xGGS linker connect the FLAG tag to the four isoforms. The construct was validated via genomic PCR and sequencing. A 3xP3-DsRed selection marker was used to facilitate genetic screening for successful knock-in validation and was excised using PiggyBac transposase.

Structural models

Dr. Kempf, a previous postdoc in the Miesenböck group, created the predicted structural model of Hyperkinetic isoform RE using Phyre2 (Kelley et al., 2015). The structural data file for $K_v\beta2$ was obtained from the Research Collaboratory for Structural Bioinformatics Protein Data Bank (1ZSX). Structures were visualized in PyMOL.

Bacterial expression and purification of His-tagged constructs

The sequence for Hyperkinetic isoform RE was subcloned into a pNIC28-Bsa4 vector with an N-terminal His tag. BL-21(DE3) bacteria containing the plasmids with Hyperkinetic wild-type and various mutants were grown in terrific broth at 37 °C and induced with 1 mM isopropyl β-D-thiogalactopyranoside at 18 °C for 16 hours. Cells were harvested via centrifugation at 5,000 RPM for 20 minutes at 4 °C. Throughout the purification process, a 500 mM NaCl, 20 mM Tris, pH 7.9 buffer was used. Cells were lysed in buffer supplemented with 5 mM imidazole with a sonication probe using 80% amplitude with 5 seconds on and 5 seconds off for 12 minutes and then centrifuged at 14,000 RPM for 1 hour. The supernatant was then incubated with Ni resin (Ni Sepharose 6 Fast Flow) on a shaking incubator for 1 hour at 4 °C before being loaded on a column pre-equilibrated with buffer and washed 3 times with a 5 mM imidazole buffer (Tipparaju et al., 2008). The resin was then 3 times with a 20 mM imidazole buffer to wash non-specifically bound proteins before the protein was eluted with a 300 mM imidazole buffer and loaded on a size exclusion column pre-equilibrated with reaction

buffer (Weng et al., 2006). Fractions containing the protein of interest were then concentrated.

Multiple turnover enzymatic assay

The steady-state multiple turnover assay used measures the NADPH steady-state turnover rate for Hyperkinetic with different concentrations of substrate. To assess this, absorbance at 340 nm, which indicates free NADPH and not bound NADPH or NADP+ (Weng et al., 2006; Tipparaju et al., 2008), was monitored on a PHERAstar FSX plate-reader at 25 °C. Depletion of free NADPH was then monitored over time to determine the steady-state NADPH turnover rate. Each well contained 50 uL of total reaction volume: 600 uM NADPH, 10 uM enzyme, and the desired concentration of substrate in a 0.2 M potassium phosphate buffer, pH 7.4 (Tipparaju et al., 2008). Turnover rate calculations were background subtracted and normalized to the no substrate condition to control for any potential confounding absorbance signals.

Statistical analysis

Data were analyzed in Prism 9 (GraphPad) and statistical details are included in the relevant figure captions.

Results chapter 1: Mass spectrometry (MS) characterization of $K_v\beta2$ native ligands

Introduction

The aim of this chapter was to identify $K_v\beta2$'s native ligands since it is currently unknown what substrates natively bind to and thus regulate $K_v\beta$ subunits, as indicated by the unresolved electron density overlying $K_v\beta2$'s active site in the purified $K_v1.2$-$K_v\beta2$ complex (Figure 3) (Long et al., 2005). This knowledge would lead to a better understanding of the cellular role and regulation of $K_v\beta$ subunits and their corresponding ion channel binding partners, particularly in the context of sleep regulation, through which $K_v\beta$ substrates could potentially serve as sleep-regulatory drugs (Kempf et al., 2019). Since it is unknown what substrates natively regulate $K_v\beta$ subunits, insight into this could further elucidate how $K_v\beta$ subunits mediate the interactions between specific cellular processes that affect cellular redox states and altered membrane excitability (Gulbis et al., 1999, Gulbis et al., 2000; Kempf et al., 2019).

Work done in this chapter focused on $K_v\beta2$ and not other $K_v\beta$ subunits because extensive work has focused on $K_v\beta2$ substrates (Long et al., 2005; Weng et al., 2006; Tipparaju et al., 2008). Importantly, potential native substrates for other $K_v\beta$ subunits have not been reported for any other $K_v\beta$ subunit except for $K_v\beta2$ (Long et al., 2005), establishing $K_v\beta2$ as a suitable starting point for native ligand identification to optimize methodological approaches before trying similar approaches on other $K_v\beta$ subunits for which native ligand information is lacking. Long et al. (2005) raise the possibility that the unresolved electron density could be from a polypeptide or an organic molecule.

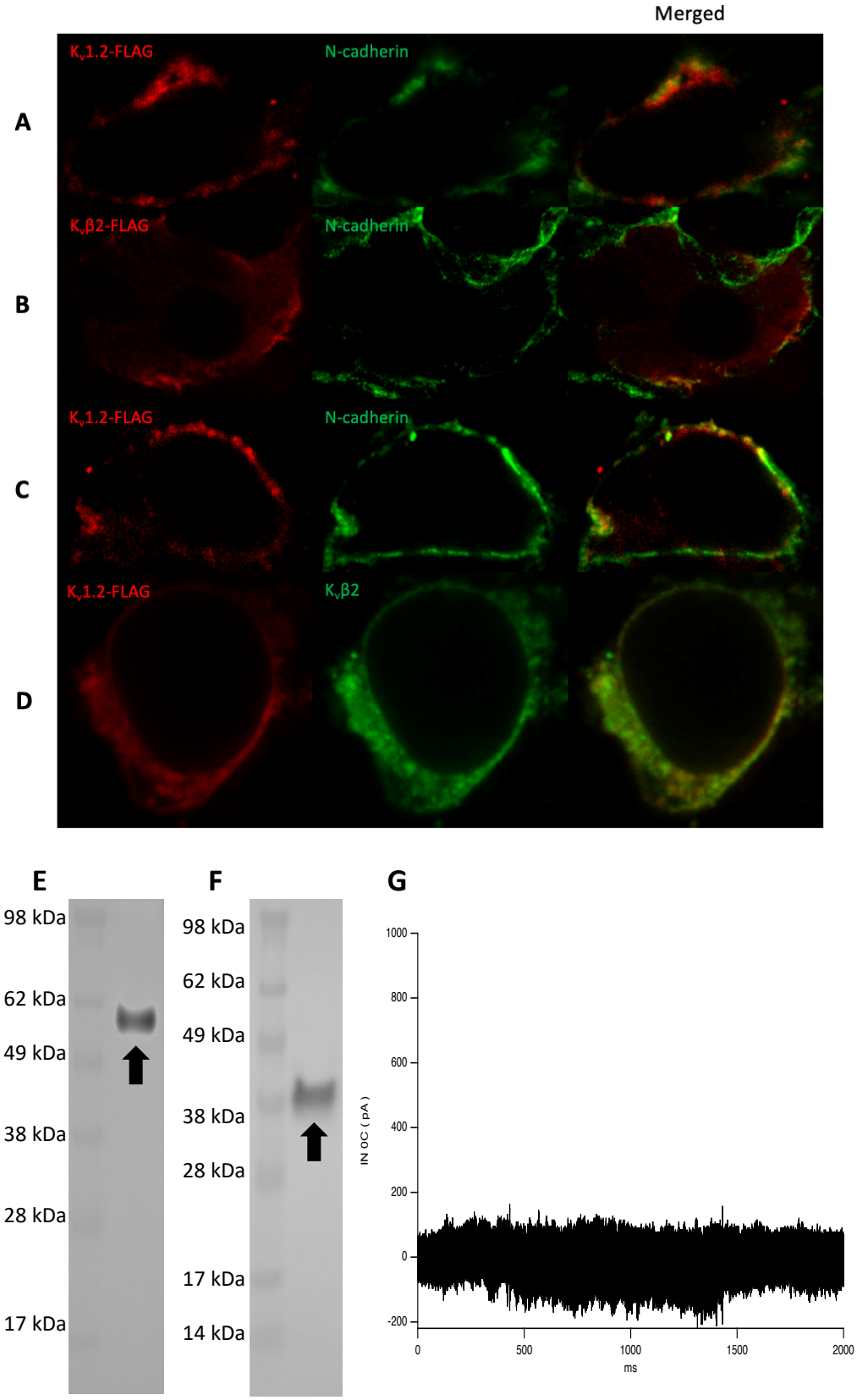
Further work has shown that $K_v\beta2$ has high specificity for reducing aldehyde- and ketone-containing organic molecules, many of which are lipid peroxidation products (Weng et al., 2006; Tipparaju et al., 2008; Xie et al., 2011). Furthermore, given the short half-life of ROS and the role of Hyperkinetic in coupling mitochondrial ROS production to altered membrane excitability through its catalytic functions (Kempf et al., 2019), it is possible that mitochondrial ROS reacts locally with lipids to release more stable lipid peroxidation products that serve as native substrates of $K_v\beta$ subunits at the plasma membrane. Indeed, $K_v\beta2$ can reduce the oxidized breakdown products of lipids *in vitro*, as demonstrated via MS characterization of the heterogenous reduced products stemming from $K_v\beta2$ reaction with oxidized breakdown products of PAPC, a common phospholipid (Xie et al., 2011).

Through ionization of molecules and subsequent separation based on the mass to charge ratio, MS is a highly sensitive and specific technique that can be used to study subtle mass differences in a heterogenous mix, as demonstrated by characterization of multiple substrates related to lipid breakdown (Xie et al., 2011). Recent advancements in native MS technology, which allows for intact protein-ligand complexes to be observed and studied in their native state, have made it possible to achieve better resolution in understanding endogenous ligand interactions with proteins (Mehmood et al., 2015; Robinson, 2019). Indeed, native MS is now able to accurately identify native ligands, even on membrane protein complexes (Gault et al., 2020), which provides a significant advancement for better understanding unresolved electron densities (Long et al., 2005; Li et al., 2015; Smart et al., 2018). As such, a collaboration with the Robinson group, experts in native MS, was formed to study the native ligands of $K_v\beta2$.

Soluble $K_v\beta2$ was tested first used instead of the $K_v1.2$-$K_v\beta2$ complex to first optimize an approach to navigating the challenge of identifying unknown endogenous ligands. If successful, a similar approach can be employed to study $K_v\beta$ subunit native ligands when bound to $K_v\alpha$ subunits, which are more difficult to study given the complexity of purifying intact membrane protein complexes (Long et al., 2005). Indeed, Long et al. (2005) used multiple lipids and detergents in order to extract the ion channel complex, which could potentially represent the molecules in the unresolved electron density. To address this potential concern, no exogenous lipids or detergents were used in purifying the soluble $K_v\beta2$. Following MS experiments of the purified soluble $K_v\beta2$, initial MS experiments were also conducted on the $K_v1.2$-$K_v\beta2$ complex, which had to be extracted with exogenous DDM, to confirm whether additional masses could also be seen on the $K_v1.2$-$K_v\beta2$ complex Long et al. (2005) studied.

Verification and purification of $K_v\beta2$ construct

Prior to identifying $K_v\beta2$'s native ligands, the mouse $K_v\beta2$ construct used was tested for its localization, catalytic activity, and regulation of A-type currents. As expected, when overexpressed by itself, $K_v\beta2$ is found in the cytoplasm, but in the presence of an alpha subunit, $K_v\beta2$ is located at the plasma membrane, as indicated by its colocalization with N-cadherin (Figure 4A-D). Western blot staining of a FLAG immunopurified $K_v1.2$-FLAG-$K_v\beta2$ complex confirmed that $K_v\beta2$ binds to $K_v1.2$ at the plasma membrane (Figure 4E, F). As further verification, $K_v\beta2$ is a functional enzyme bound to NADPH (Figure 5) and regulates A-type current inactivation (see results chapter 2).


Merged
A
K_v1.2-FLAG
N-cadherin
B
K_vβ2-FLAG
N-cadherin
C
K_v1.2-FLAG
N-cadherin
D
K_v1.2-FLAG
K_vβ2
E
98 kDa
62 kDa
49 kDa
38 kDa
28 kDa
17 kDa
F
98 kDa
62 kDa
49 kDa
38 kDa
28 kDa
17 kDa
14 kDa
G
IN 0C (pA)
1000
800
600
400
200
0
-200
0
500
1000
1500
2000
ms

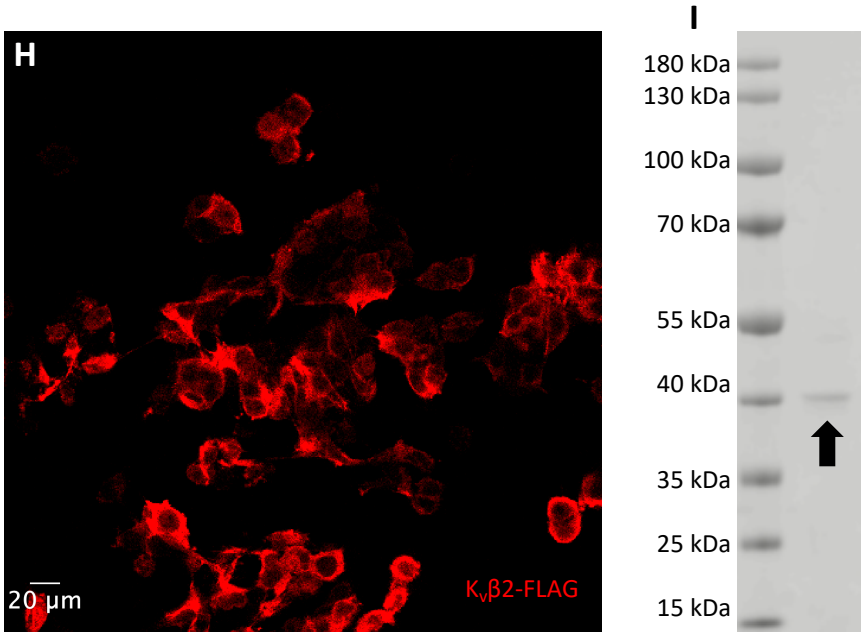


Figure 4. Verification and purification of $K_v\beta2$ construct

(A) Representative confocal image of a HEK-293 cell transfected with $K_v1.2$-FLAG (C-terminal) and stained with antibodies against FLAG (red) and N-cadherin (green).

(B) Representative confocal image of a HEK-293 cell transfected with $K_v\beta2$-FLAG (C-terminal) and stained with antibodies against FLAG (red) and N-cadherin (green).

(C) Representative confocal image of a HEK-293 cell transfected with $K_v1.2$-FLAG (C-terminal) and $K_v\beta2$ and stained for FLAG (red) and N-cadherin (green).

(D) Representative confocal image of a HEK-293 cell transfected with $K_v1.2$-FLAG (C-terminal) and $K_v\beta2$ and stained for FLAG (red) and $K_v\beta2$ (green).

(E) $K_v1.2$-FLAG-$K_v\beta2$ was expressed in HEK-293 cells (same as (D)), FLAG immunopurified, and stained for FLAG in a Western blot. The FLAG signal that corresponds to Kv1.2-FLAG, which has a molecular weight of ~60 kDa, falls between 62 kDa and 49 kDa.

(F) Same as (E) but stained for $K_v\beta2$ with a anti-$K_v\beta2$ antibody. The $K_v\beta2$ signal falls between 49 kDa and 38 kDa. $K_v\beta2$ has a molecular weight of ~41 kDa.

(G) Composite graph of evoked currents form untransfected HEK-293 cells in a voltage clamp recording from -100 mV to 50 mV.

(H) Representative confocal image (stained for FLAG) of a stable cell line of HEK-293 cells expressing $K_v\beta2$-FLAG (C-terminal) with the first N-terminal 35 amino acids removed.

(I) Coomassie gel of eluted protein from a large-scale FLAG immunopurification from the stable cell line in (H). The construct has a molecular weight of ~41 kDa, and the band sits at the 40 kDa ladder mark. This Coomassie gel was run and imaged by collaborators in the Robinson group.

Although HEK-293 may natively express $K_v\beta2$ and several $K_v\alpha$ ion channels (Jiang et al., 2002), no $K_v\beta2$ antibody signal was seen on untransfected cells, and voltage clamp recordings from untransfected cells showed no current responses (Figure

4G). Moreover, overexpressed cytoplasmic $K_v\beta2$ is spread throughout the cytoplasm and is not membrane-localized (Figure 4B). These results suggest that native $K_v\beta$ and $K_v\alpha$ expression, if any, in the HEK-293 used in this thesis is minimal and not detectable.

Following functional verification of the $K_v\beta2$ construct, a purification protocol was optimized. To avoid protein aggregation for large-scale purifications, the first 35 N-terminal amino acids of $K_v\beta2$ were removed (Gulbis et al., 1999). A large-scale purification with no exogenous lipids or detergents of this construct from a stable cell line yielded a pure and specific product suitable for MS analysis: only the oligomeric $K_v\beta2$ species was detected in the highly sensitive native MS experiments (Figure 4H, I; Figure 6A). Proteomics analysis was conducted on the eluted product and confirmed the protein product and purity. No peptides corresponding to the first 35 amino acids of human $K_v\beta2$ were found, suggesting that even if native $K_v\beta2$ were expressed in the HEK-293 cells used, they were not incorporated into the overexpressed FLAG-tagged protein product that was purified.

Purified $K_v\beta2$ is a functional enzyme predominantly bound to NADPH

All MS experiments that follow were done by collaborators in the Robinson group. I assisted with experimental planning and data analysis, and they prepared all the figures.

To determine the oxidation state of $K_v\beta2$'s cofactor, the protein was boiled to release its cofactor. MS analysis revealed that the released cofactor is predominantly NADPH (Figure 5A). Given this, purified $K_v\beta2$ should be able to reduce substrates without exogenous NADPH. Indeed, when incubated with just POVPC, a lipid

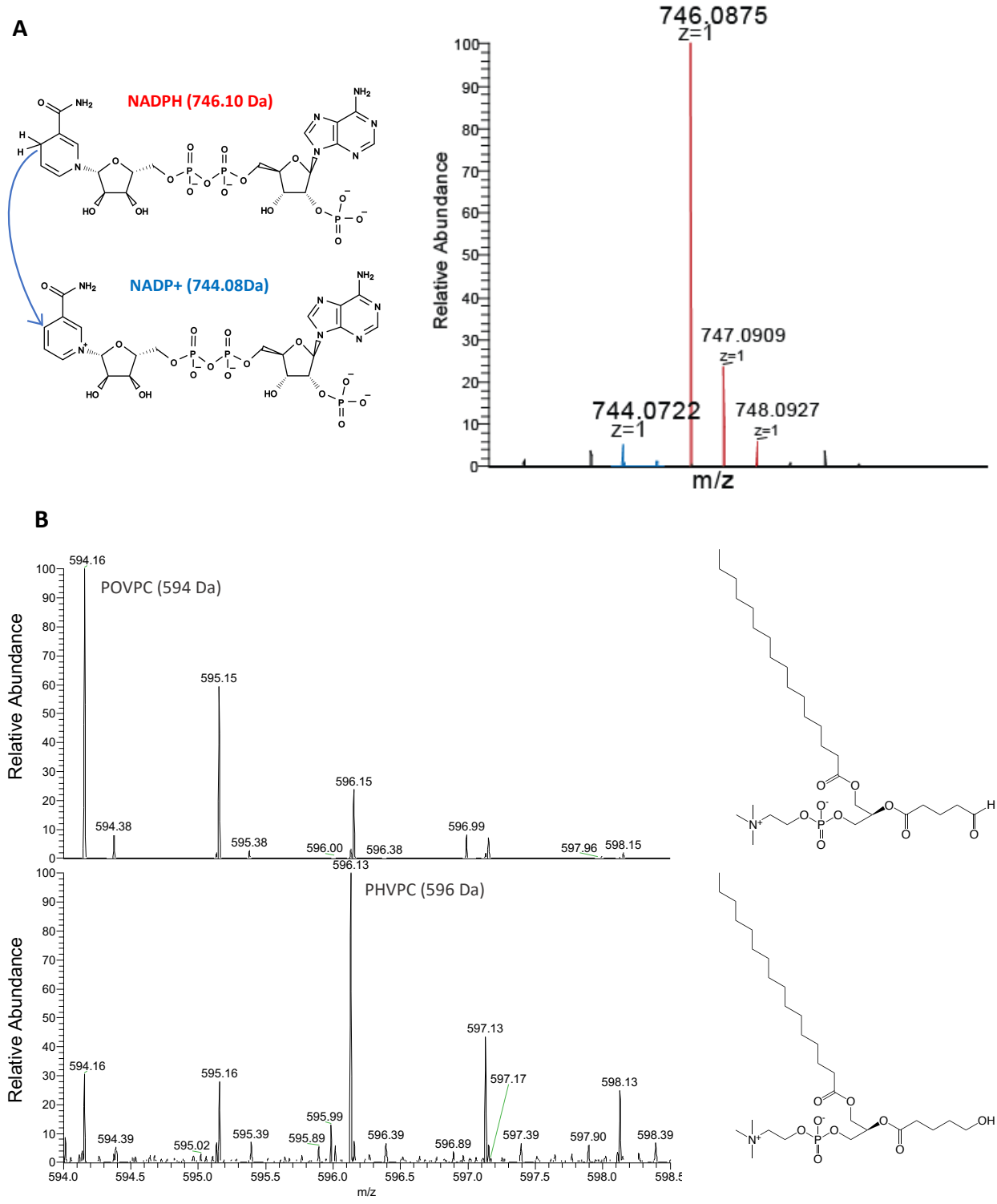


Figure 5. $K_v\beta2$ is a functional enzyme predominantly bound to NADPH

(A) (Left) Structures of NADP+ and NADPH demonstrating their mass difference. (Right) MS spectrum of the released cofactor from $K_v\beta2$. NADP+ inherently has a +1 charge to yield a z=1, whereas NADPH needs to pick up a H+ [NADPH+H+] to give a z=1.

(B) (Top) MS spectrum of POVPC (1-palmitoyl-2-oxo-valaroyl-3-phosphotidyl choline) incubated without $K_v\beta2$. Structure of POVPC with its aldehyde group (right-most part of the structure) shown on the right. (Bottom) MS spectrum of POVPC incubated with $K_v\beta2$ demonstrates that POVPC was reduced to PHVPC (1-palmitoyl-2-hydroxyvaleroyl phosphatidylcholine). Structure of PHVPC with its alcohol group (right-most part of the structure) on the right.

peroxidation product (Parvez et al., 2018) known to react with $K_v\beta2$ (Tipparaju et al., 2008), it reduced it to PHVPC (Figure 2B), further validating the $K_v\beta2$ construct as a functional enzyme.

Native MS reveals additional masses bound to $K_v\beta2$

Under native MS conditions, the observed mass corresponds to a $K_v\beta2$ octameric complex with 8 bound NADPH cofactors and a heterogenous mix of additional masses that may indicate native ligands (Figure 6A). At higher HCD energies that dissociate bound NADPH cofactors and potential ligands, the observed mass of 327,369$\pm$252 Da (Figure 6A) corresponds to the theoretical octameric mass of $K_v\beta2$-FLAG, 327,280.4 Da, further indicating that no potentially endogenous $K_v\beta2$ was incorporated. No other oligomeric states were observed. To ensure that the additional masses were not due to non-specific binding to the FLAG tag, GFP with an identical C-terminal FLAG tag was also purified from HEK-293 cells. Native MS analysis of GFP-FLAG revealed only sharp peaks with no additional masses (Figure 6B).

Small molecular weights detected on $K_v\beta2$

To provide higher resolution of the heterogenous mix of additional masses bound to the octameric $K_v\beta2$, urea was added to dissociate monomeric subunits along with cofactors and native ligands (Figure 7A-C). The concentrations of urea used (100-500

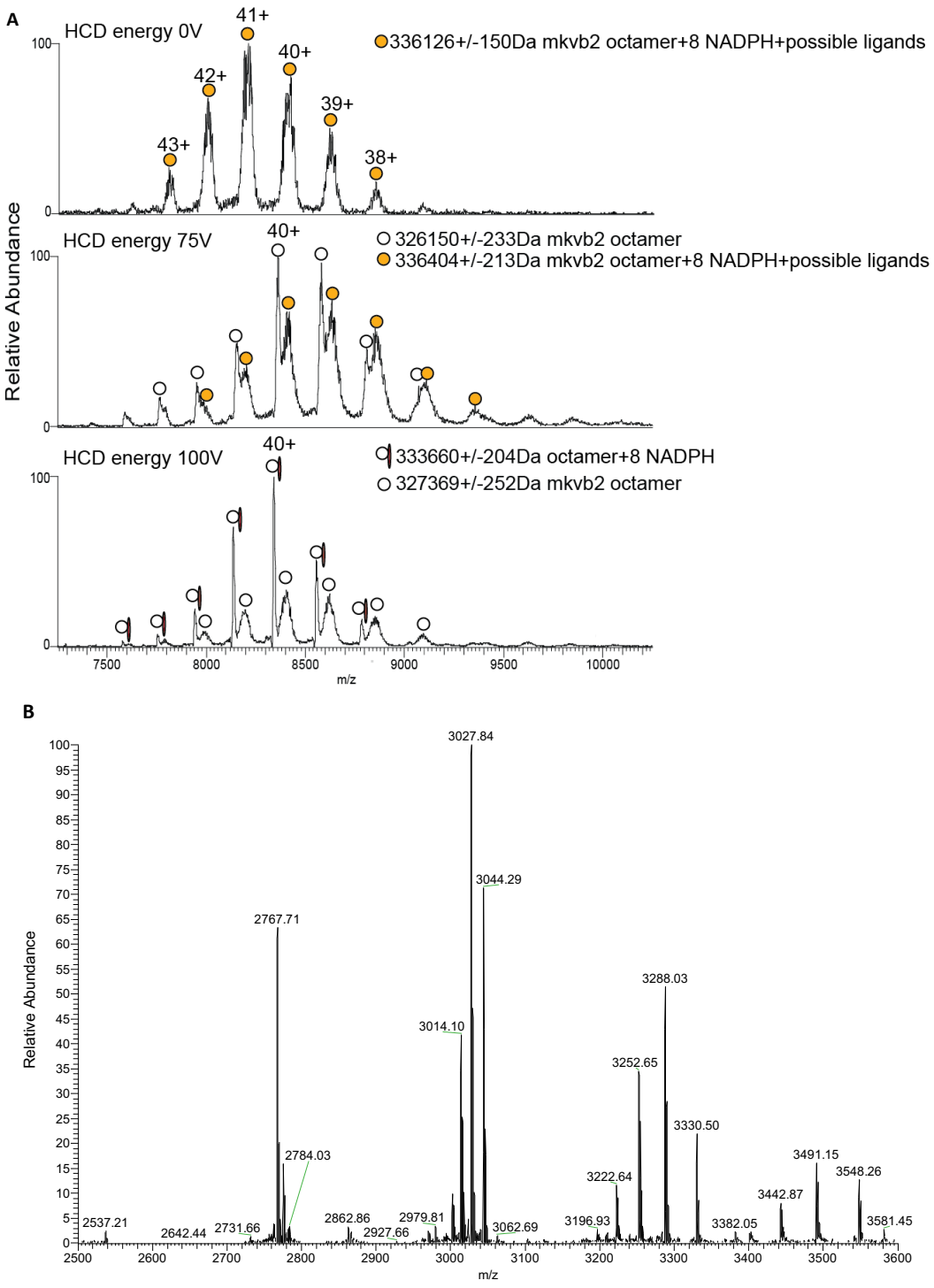


Figure 6. Native MS reveals additional masses bound to $K_v\beta2$

(A) Native MS spectra of $K_v\beta2$-FLAG at various higher energy collision dissociation (HCD) energies reveal bound cofactors and additional masses. Three different energies (0, 75 and 100 V) were used to dissociate the cofactors and ligands to observe the subsequent mass shift to identify the mass of the potential ligands and the mass of the protein without any bound cofactors and ligands.

(B) Native MS spectrum of GFP-FLAG reveals no additional masses.

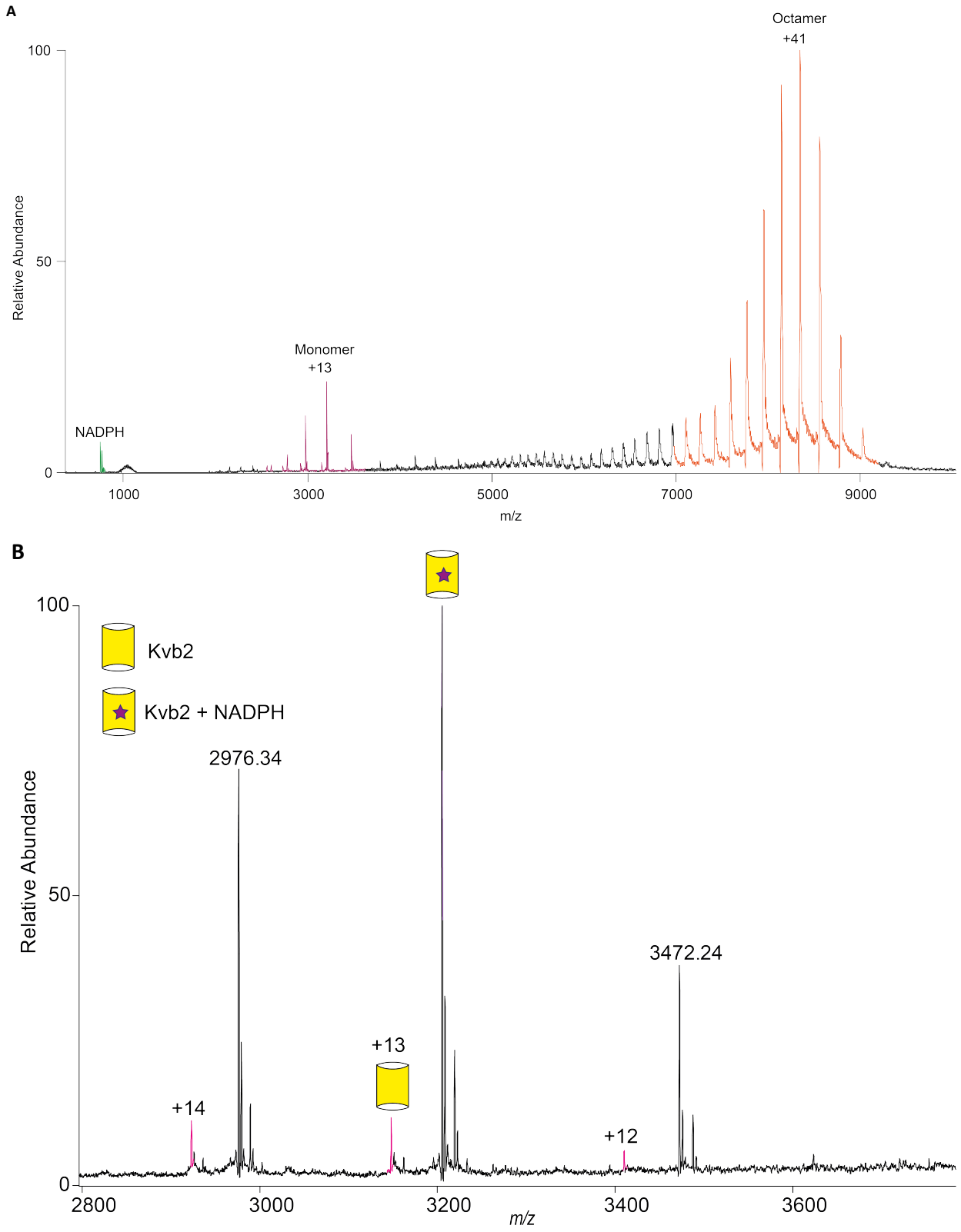
mM) were titrated from a stock solution until the concentration was sufficient to observe dissociated monomeric subunits, cofactors, and potential ligands (Figure 7). At concentrations higher than 500 mM urea, signals in the small molecule range were suppressed. In the dissociated monomeric and small molecule range, NADPH was found in high abundance (Figure 7B, C). Various small molecules were present in lower abundance in the 700-800 Da range (Figure 7C). Due to low concentrations and ligand heterogeneity, it was not possible to definitively determine the identity of these molecules; however, the 812.04 and 828.01 peaks (Figure 7C) closely align with the masses observed for 2H-PECPC and PEIPC, respectively, products generated from air oxidation breakdown of the lipid PAPC and known to have reactivity with $K_v\beta2$ (Xie et al., 2011).

POVPC does not stably bind to $K_v\beta2$

To test whether exogenous lipid peroxidation products would stably bind to $K_v\beta2$ so that they could be detected on MS, $K_v\beta2$ was incubated with POVPC and analyzed on MS. Although $K_v\beta2$ is capable of reducing POVPC (Figure 5B), it does not stably bind to it long enough to be detected on MS (Figure 8). This suggests that endogenous lipid peroxidation products from HEK-293 cells that may serve as native regulators of $K_v\beta$ subunits may not stably bind for long enough during the purification process to still be in the active site for later MS analysis.

Dissociated $K_v\beta2$ from the $K_v1.2$-$K_v\beta2$ complex has additional masses

To see if the membrane-localized $K_v\beta2$ complexed with an alpha subunit has


A
Octamer
+41
100
Relative Abundance
50
Monomer
+13
NADPH
0
1000
3000
5000
7000
9000
m/z
B
100
Kvb2
Kvb2 + NADPH
2976.34
Relative Abundance
50
3472.24
+13
+14
+12
0
2800
3000
3200
3400
3600
m/z

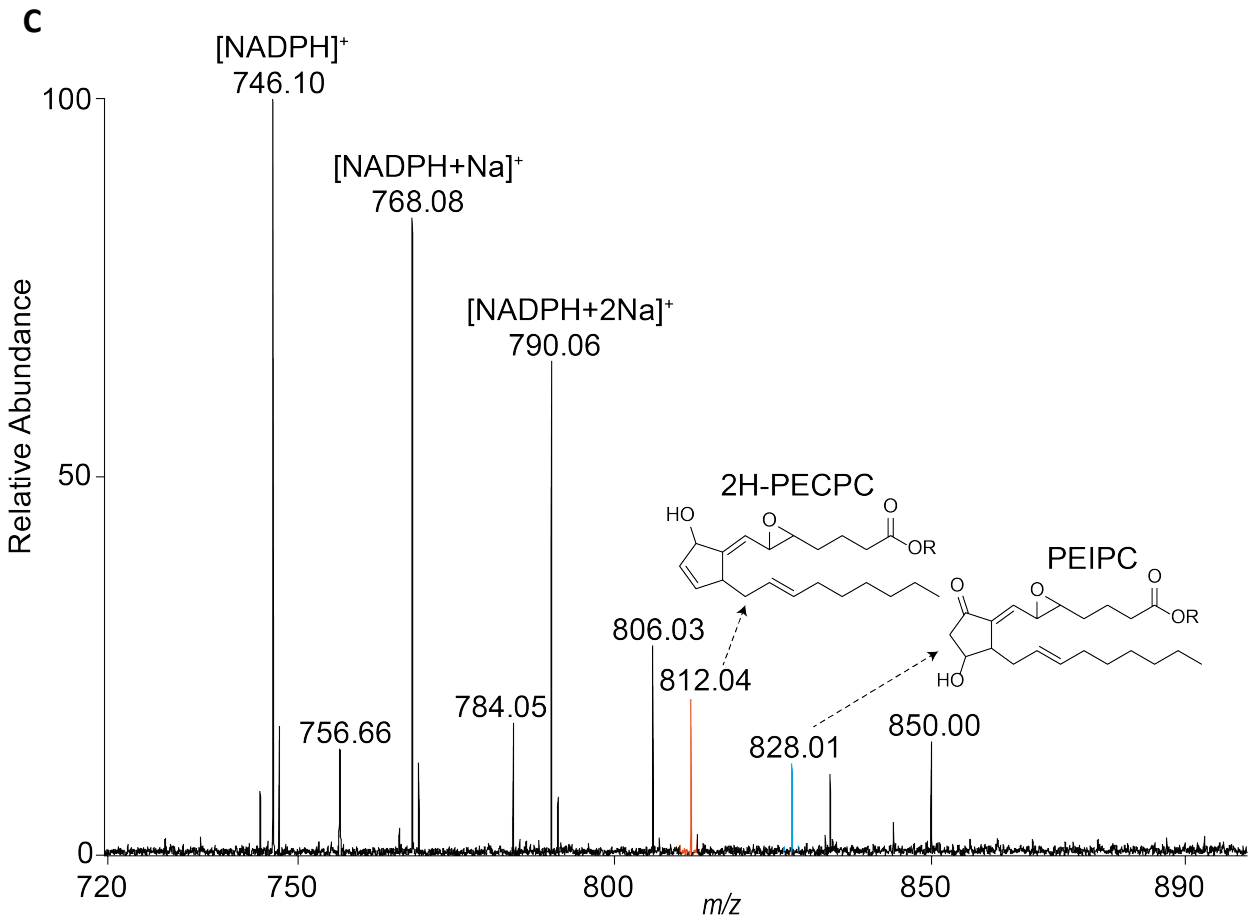


Figure 7. Small molecular weights detected on $K_v\beta2$

(A) Electrospray ionization (ESI) spectrum of $K_v\beta2$ with 500 mM urea.
(B) ESI spectrum of the monomeric region of $K_v\beta2$ with 500 mM urea.
(C) ESI spectrum of the small molecule region of $K_v\beta2$ with 100 mM urea. The 812 Da peak might correspond to 2H-PECPC (shown in figure inlet), which is the reduced form of PECPC (1-palmitoyl-2-(epoxycyclopentenone)-*sn*-glycero-3-phosphorylcholine), and the 828 Da peak might correspond to PEIPC (shown in figure inlet) (1-palmitoyl-2-(5,6)-epoxyisoprostane E2-*sn*-glycero-3-phosphocholine).

additional masses that might correspond to native ligands, the full $K_v1.2$-$K_v\beta2$ complex was purified from a detergent extract and $K_v\beta2$ was dissociated from the integral membrane portion of the channel (Figure 4E, F) and analyzed on native MS (Figure 9). Interestingly, the dissociated $K_v\beta2$ was also present only as an octamer. Similar to the soluble $K_v\beta2$ purified without any exogenous lipids added during the purification

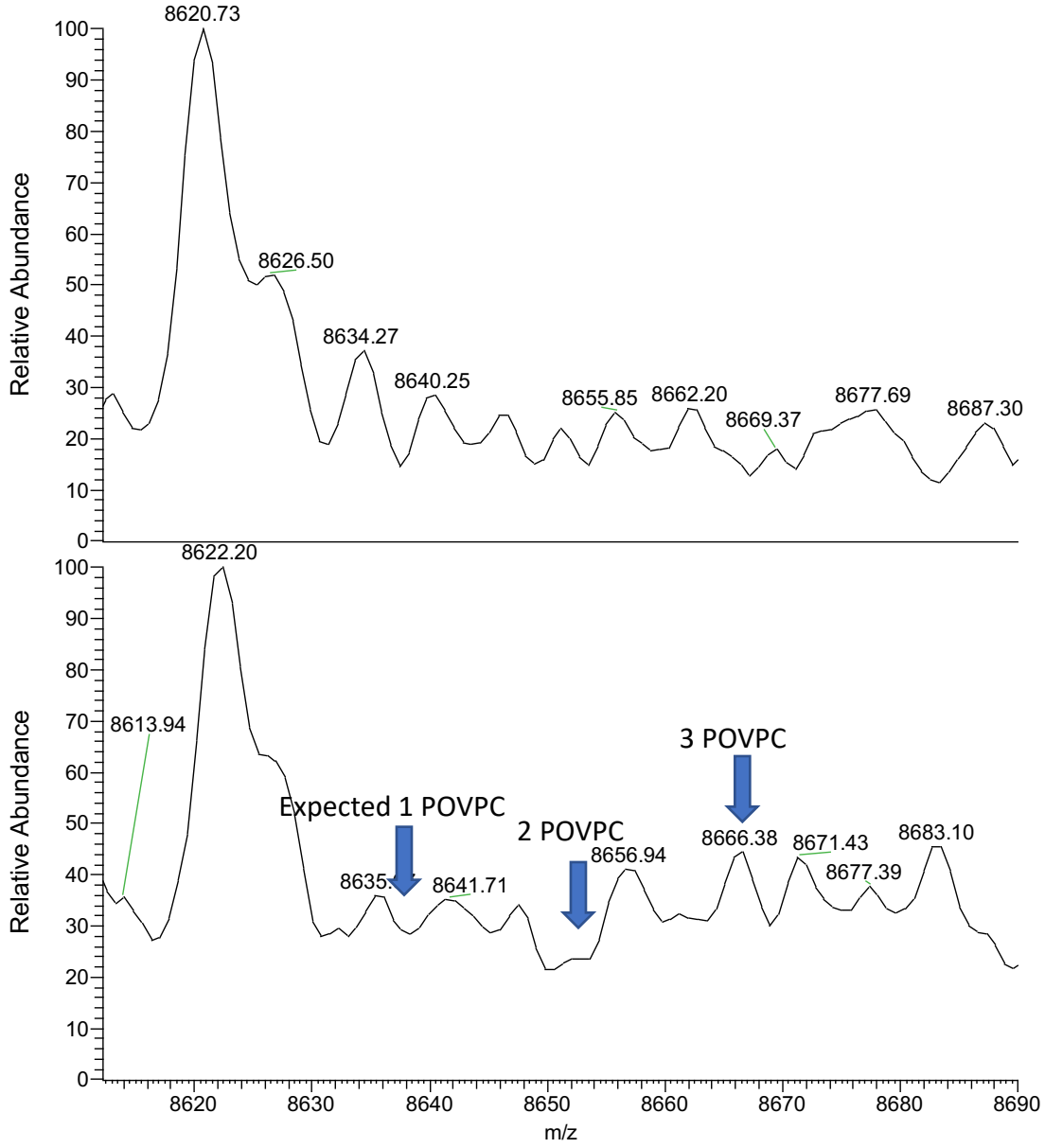


Figure 8. POVPC does not stably bind to $K_v\beta2$. (Top) Native MS spectrum of $K_v\beta2$ with no added substrates. (Bottom) Native MS spectrum of $K_v\beta2$ incubated with POVPC with arrows indicating areas where expected peaks for POVPC binding would be detected. This was an independent experiment and the data shown here are not from a previous figure. MS conditions were optimized at minimal activation energy to maintain the integrity of potential ligand-protein binding.

process, the membrane-localized $K_v\beta2$ dissociated from its alpha subunit, which was purified using the detergent DDM, also had additional masses beyond that of bound NADPH (Figure 9). The additional masses that correspond to potential ligands are

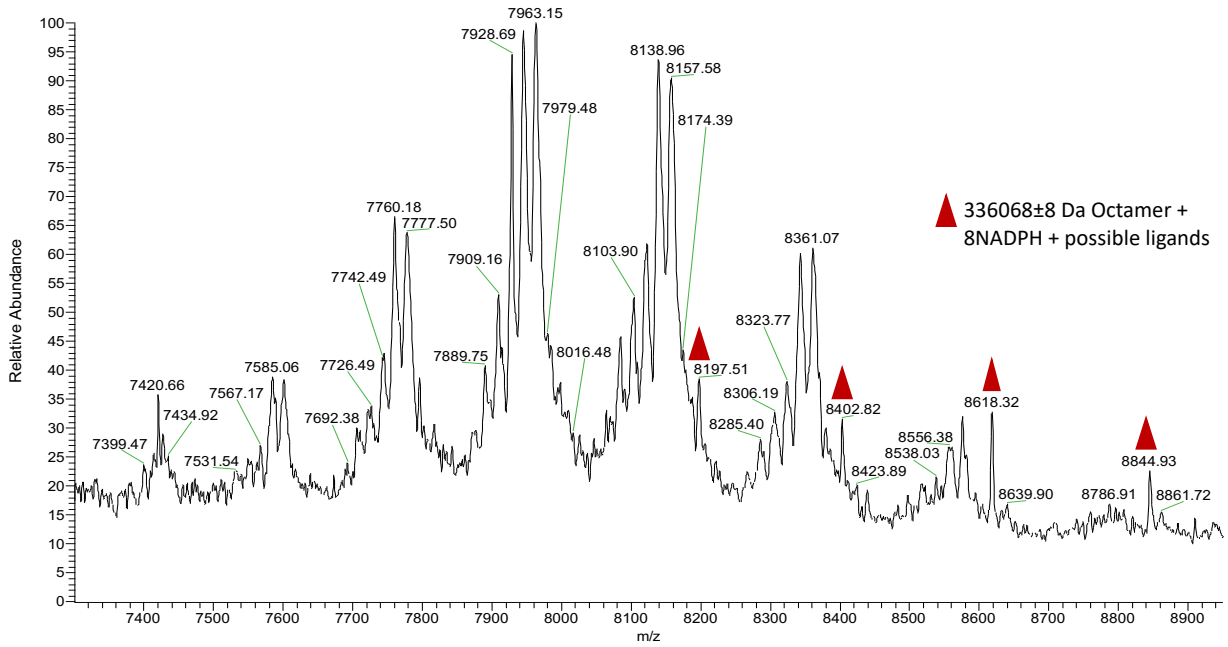


Figure 6. Dissociated $K_v\beta2$ from the $K_v1.2$-$K_v\beta2$ complex has additional masses. Native MS spectrum of $K_v\beta2$ dissociated from the $K_v1.2$-$K_v\beta2$ complex using HCD energy of 200 V. The charge state of the central cluster of peaks (7963.15) has a charge state of 42+. The mass of the potential ligands observed is around 1.5 kDa.

around 1.5 kDa. However, due to contaminants from purifying a membrane-localized protein and the presence of alpha subunits in the spectra, it was not possible to achieve better resolution of the additional masses on the dissociated $K_v\beta2$.

Discussion

In response to elevated ROS signals in the dFB during waking, Hyperkinetic subunits coupled to Shaker register this via oxidative conversion of their NADPH cofactors to NADP+, which help drive the fly to sleep when the relevant sleep signals arrive (Kempf et al., 2019). Indeed, it was found that purified $K_v\beta2$ is predominantly bound to NADPH (Figure 5A), and this pool of bound reduced cofactors would gradually become oxidized as ROS signals accumulate. In this manner, the oxidative state of $K_v\beta$ subunits' cofactors influences sleep through their regulatory role on A-type potassium

currents. However, it is unknown what substrates natively regulate $K_v\beta$ subunits in this context. An unresolved electron density in the active site of $K_v\beta2$ in a purified $K_v1.2$-$K_v\beta2$ complex suggests the possibility of a heterogenous mixture of native ligands (Long et al., 2005). Furthermore, given the instability of ROS products and $K_v\beta2$'s ability to reduce lipid peroxidation products, it may be possible that lipid peroxidation products generated locally from ROS reactions serve as the intermediary signaling link between elevated ROS signals and conversions to NADP+ (Xie et al., 2011; Tipparaju et al., 2008).

As such, the primary aim of this chapter was to uncover $K_v\beta2$'s native ligands. Knowledge about $K_v\beta$ subunits' endogenous ligands would provide critical information about how K_v ion channels are natively regulated through $K_v\beta$ subunits in the context of cellular redox. This information would then further facilitate drug screens to identify potential sleep drugs given $K_v\beta$ subunits' role in sleep regulation (Kempf et al., 2019).

To address the possibility that the unresolved electron density may stem from the mixture of detergents and lipids used throughout the purification process (Long et al., 2005), $K_v\beta2$, the soluble portion of the ion channel complex (Figure 4B), was first purified from HEK-293 cells without exogenous lipids. Cell lysis was achieved via sonication to avoid using detergents. Therefore, the additional masses found on $K_v\beta2$ are not artifacts from the purification process, which is further confirmed by a different soluble construct purified via the same immunopurification process targeting the same FLAG epitope not having any additional masses (Figure 6).

The additional masses found on $K_v\beta2$ were indeed a heterogenous mixture (Figures 6, 7); however, it was not possible to conclusively verify the identity of the small

molecule ligands detected. It is important to note, however, that the masses of the stably bound ligands that were detected were within the 700-900Da range, which corresponds to the mass expected for certain lipid peroxidation products (Parvez et al. 2018; Xie et al., 2011). To conclusively match the identity of the small molecule ligands with confirmed structures, however, MS fragmentation spectra of pure compounds for the predicted molecules would be needed to compare with the fragmentation spectra of the unidentified masses, but these cannot be commercially purchased. They are also difficult to produce in sufficient yields and purity due to the heterogenous mixture of breakdown products created when lipids become oxidized (Xie et al., 2011).

Thus, as it stands, the molecular identities of the currently unidentified ligands (Long et al., 2005; Figures 6, 7, 9) remain unknown, but more is now known about them. Critically, the masses of several of the molecules have been identified, which can help narrow down the search for what they might be, and it is known that the masses represent a heterogenous mix. It is also now known that the unidentified masses are most likely native ligands and not byproducts from the purification process. It is possible that the unresolved electron density found in Long et al. (2005) and the additional masses reported here span different chemical identities due to different cells used to create the protein (Long et al., 2005 used *Pichia pastoris*) and due to the different cellular positions of $K_v\beta2$, either complexed with $K_v1.2$ at the plasma membrane in close proximity to the lipid bilayer or soluble throughout the cytoplasm. Interestingly, additional masses were also observed on $K_v\beta2$ from a purified $K_v1.2$-$K_v\beta2$ complex, though the spectral resolution for the dissociated $K_v\beta2$ was not as ideal (Figure 9). Thus, before identifying the native ligands on the full ion channel complex, a method must be

optimized to accurately identify the molecules in the heterogenous mix of ligands found on the soluble $K_v\beta2$.

It is also possible that many native ligands were lost during the purification process, especially smaller lipid peroxidation molecules that are unstable, such as 4-ONE. Even though these molecules may natively regulate $K_v\beta2$ and influence A-type inactivation (see results chapter 2), they may not stably bind for long enough to be detected on MS, as was the case with POVPC, which was capable of being reduced by $K_v\beta2$ but was not detected as stably bound to $K_v\beta2$ (Figure 8).

Results chapter 2: $K_v\beta2$'s influence on A-type current inactivation

Introduction

If lipid breakdown products natively regulate $K_v\beta$ subunits, they should be able to act through $K_v\beta$ subunits to delay A-type current inactivation. It has previously been shown that 4-cyanobenzaldehyde, an aldehyde-containing molecule, can influence $K_v1.4$ currents through $K_v\beta2$ (Weng et al., 2006), but this effect has not been demonstrated with lipid peroxidation products. Furthermore, previous work has shown that cofactor oxidation can be modulated by voltage (Pan et al., 2008a), and current work in the lab has demonstrated that Hyperkinetic cofactor exchange can be accelerated through membrane depolarization (unpublished). As such, the aims of this chapter were two-fold: (1) to investigate how $K_v\beta2$ modulates A-type current inactivation through lipid peroxidation products, and (2) to test whether $K_v\beta2$ cofactor exchange can be accelerated through voltage changes.

To test these aims, a reconstituted ion channel expression system in HEK-293 cells was established since the HEK-293 cells used in lab do not have detectable currents in voltage clamp (Figure 4G) and since HEK-293 cells have been used to study the electrophysiological properties of K_v ion channels (Faivre et al., 1999). As such, HEK-293 cells are a suitable system to transiently express $K_v1.4$, which has characteristic A-type currents (Weng et al., 2006), concurrently with $K_v\beta2$ to test A-type current modulation in the context of lipid peroxidation product regulation through $K_v\beta2$. $K_v1.4$ was used in this chapter since its characteristic A-type currents resemble Shaker's A-type currents (Weng et al., 2006; Hoshi et al., 1990; Zagotta et al., 1990)

that are modulated by Hyperkinetic redox regulation (Kempf et al., 2019). As such, studying $K_v\beta2$ regulation of $K_v1.4$ would provide better insight into how lipid peroxidation products may natively regulate Hyperkinetic and Shaker in the context of sleep.

Previous biochemical studies have identified lipid peroxidation products, such as 4-ono-2-nonenal (4-ONE), which has both aldehyde and ketone functional groups, that demonstrate reactivity with $K_v\beta2$ (Tipparaju et al., 2008; Parvez et al., 2018; Esterbauer et al., 1991). Though 4-ONE is a highly reactive protein cross-linker (May-Zhang et al., 2019) that is neurotoxic at low concentrations (Lin et al., 2005), it can be reduced by $K_v\beta2$ (Tipparaju et al., 2008), potentially dampening its harmful effects and implicating $K_v\beta2$ in a neuroprotective role (Raph et al., 2019). Indeed, it has been shown that a bacterial aldehyde reductase is able to protect against damage caused by lipid peroxidation products (Pérez et al., 2008). Furthermore, it was found to be neurotoxic at low concentrations when supplied extracellularly in cell culture media (Lin et al., 2005). Similar toxic results were observed when conducting experiments for this thesis when 4-ONE was added to the extracellular solution for electrophysiology experiments. However, no toxic effects were observed when the same concentration of 4-ONE was used in the intracellular solution for recordings, perhaps because cells have internal mechanisms for redox homeostasis, most notably in this case the overexpression of $K_v\beta2$. Furthermore, successful recordings were able to be obtained without complications while patching with 4-ONE, suggesting that cell viability and quality were not compromised enough, if at all. Lastly, other lab members have successfully used 4-ONE in recording from fly neurons without any toxicity issues (unpublished).

However, given these potential complications, several other lipid peroxidation compounds, such as methylglyoxal and 4-hydroxy-2-nonenal (4-HNE), were tested in addition to 4-ONE—all of which represent physiologically relevant metabolites (Esterbauer et al., 1991; Wetzels et al., 2017).

$K_v\beta2$ relocates to the plasma membrane in the presence of $K_v1.4$

To test $K_v\beta2$'s influence on $K_v1.4$ inactivation, HEK-293 cells were transiently transfected with the full-length $K_v1.4$ sequence. Cells were then co-transfected with another plasmid with an IRES-EGFP construct. To test $K_v\beta2$'s influence on A-type inactivation, the full-length $K_v\beta2$ construct was subcloned upstream of the IRES-EGFP sequence, and for control cells, no construct was included upstream. Before performing electrophysiological recordings, $K_v\beta2$ localization was analyzed first. In cells expressing only $K_v\beta2$ with IRES-EGFP, the $K_v\beta2$ signal is spread throughout the cytoplasm, in contrast to the EGFP signal which can also be seen in the nucleus (Figure 10A). However, when $K_v\beta2$ is co-expressed with $K_v1.4$, $K_v\beta2$'s signal is found only at the plasma membrane, delineated by where the EGFP signal terminates, suggesting that $K_v\beta2$ binds to $K_v1.4$ at the plasma membrane (Figure 10B).

4-ONE partially prevents $K_v1.4$ inactivation

Though a previous study found that 4-cyanobenzaldehyde had no effect on $K_v1.4$ inactivation time constants (Weng et al. 2006), $K_v1.4$ oxidation in inside-out patches prevented channel inactivation (Ruppersberg et al., 1991). Therefore, 4-ONE was first tested on $K_v1.4$ only to ensure that any differences in inactivation time constants were

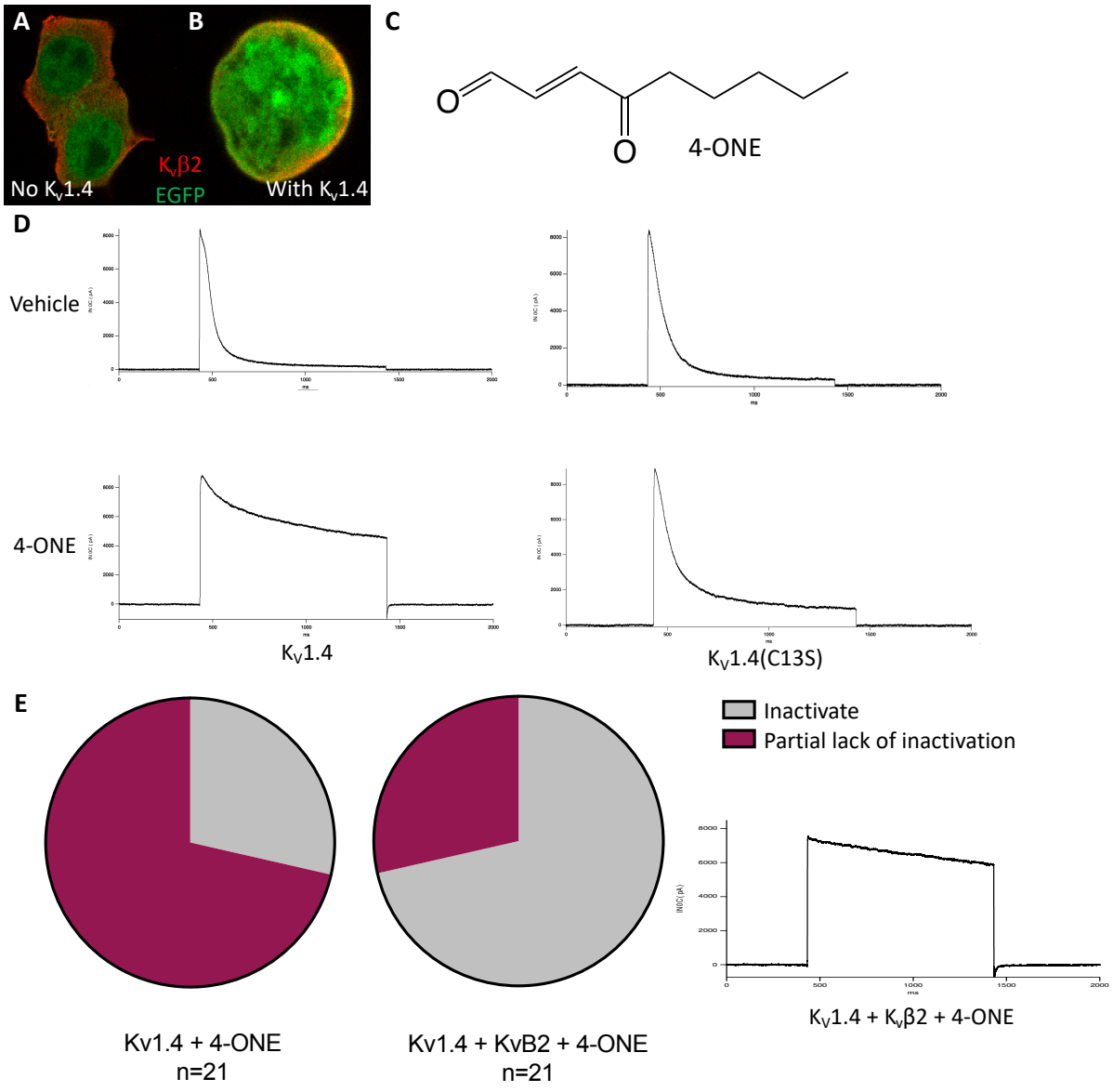


Figure 10. $K_v\beta$2 shields K_v1.4 from 4-ONE's partial lack of inactivation effect

(A) Representative confocal image of HEK-293 cells expressing $K_v\beta$2 with an IRES-EGFP construct and stained with an anti-$K_v\beta$2 antibody (red).

(B) Representative confocal image a HEK-293 cell expressing $K_v\beta$2 with an IRES-EGFP construct while simultaneously expressing K_v1.4 and stained with an anti-$K_v\beta$2 antibody (red).

(C) Chemical structure of 4-ONE.

(D) Representative current traces from single-cell voltage clamp recordings of cells expressing either K_v1.4 or K_v1.4 C13S with and without 4-ONE (100 uM).

(E) Proportion of K_v1.4 currents that either inactivate or fail to inactivate in the presence of 4-ONE based on the presence of $K_v\beta$2. A representative trace demonstrating partial lack of inactivation in the K_v1.4 + $K_v\beta$2 + 4-ONE condition is shown on the right.

not due to substrate effects on the ion channel itself. In voltage clamp recordings, K_v1.4's evoked currents showed a partial lack of inactivation in the presence of 4-ONE (Figure 10C, D). Since plasmid concentrations and time post-transfection were consistent across different days for recordings, there was no observable variability in current traces.

Since the only published instance of this phenomenon reported qualitative observations, a partial lack of channel population inactivation was defined here as the final current amplitude failing to fall below 50% of the peak current amplitude (Figure 10D) (Ruppersberg et al., 1991). Tau values as indications of inactivation time constants could not be used to quantify the partial lack of inactivation in the presence of 4-ONE since they were incalculable due to the current traces not being able to be properly fitted with a double exponential function. These results indicate that reactive electrophiles, such as 4-ONE, are capable of acting through K_v1.4 to partially prevent A-type current inactivation.

A K_v1.4 C13S mutation abolishes 4-ONE's effect on K_v1.4

A C13S mutation targeting a potential cysteine oxidation site in K_v1.4's N-terminal inactivation chain prevented the oxidative effects of inside-out patches on K_v1.4's inactivation profile (Ruppersberg et al., 1991). Similarly, a K_v1.4 C13S mutation removed all partial lack of inactivation effects due to 4-ONE (Figure 10D). Though the representative traces (Figure 10D) show a difference in the slow inactivation time constant for K_v1.4 C13S, when 4-ONE was added to the intracellular solution, there were no significant differences in the aggregate data for inactivation time constants for

K_v1.4 C13S (Figure 11A, B), thus allowing the use of this mutant to test the effect of various substrates on K_v1.4 inactivation through $K_v\beta$2.

$K_v\beta$2 shields K_v1.4 from 4-ONE's partial lack of inactivation effect

It is unknown whether $K_v\beta$ subunits can protect $K_v\alpha$ subunits from lipid peroxidation products. Since 4-ONE can influence the activity of K_v1.4, partial lack of K_v1.4 inactivation was tested in the presence of 4-ONE when $K_v\beta$2 was simultaneously expressed. $K_v\beta$2 expression decreased the percentage of currents that displayed a partial lack of inactivation in the presence of 4-ONE (Figure 10E), indicating that $K_v\beta$2 can shield K_v1.4 from 4-ONE to partially prevent modification of the inactivation peptide. Although there was some variability in the partial lack of inactivation profiles in the presence of 4-ONE, particularly in the slope of the initial inactivation in the first ~100 ms, (Figure 10E), this variability also existed among currents within the same condition, and the current magnitudes were consistently above 50% of the peak current amplitude at the end of the recordings for currents that demonstrated a partial lack of inactivation.

$K_v\beta$2 delays A-type current inactivation in a substrate-specific manner

Paul Volkmann, a rotation student, helped contribute to data collection for all the conditions in Figure 11A, B except for "C13S+B2+MeOAc", "C13S+B2+PGD2", "C13S+B2+4-HNE", "C13S+B2+4-ONE", and "C13S+B2+methylglyoxal".

Voltage-gated ion channels with characteristic A-type currents, such as Shaker and K_v1.4, undergo an initial, rapid inactivation primarily driven by N-terminal inactivation (Hoshi et al., 1990; Zagotta et al., 1990) followed by a slower, C-terminal

inactivation (Tan et al., 2022). These inactivation profiles are respectively reflected by inactivation time constants (τ_{fast} or τ_{slow}) calculated from double exponential fits of the A-type currents. Since A-type currents repolarize membrane potentials following actional potentials, modifications to their inactivation rates affect neuronal firing rates (Connor & Stevens, 1971), which has implications for sleep regulation (Kempf et al., 2019). As such, measuring inactivation time constants is critical for better understanding how A-type channels contribute to actional potential generation.

There is no significant difference in the fast or slow inactivation time constants when comparing K_v1.4 C13S with either K_v1.4 or with K_v1.4 C13S with 4-ONE (Figure 11A, B). Furthermore, there is no significant difference in inactivation time constants between K_v1.4 co-expressed with $K_v\beta$2 compared with K_v1.4 C13S co-expressed with $K_v\beta$2 (Figure 11A, B). Interestingly, when the currents that exhibited a partial lack of inactivation were removed from analysis and the remaining currents' inactivation time constants were analyzed, the resulting tau values were similar for K_v1.4 and K_v1.4 C13S in the presence of 4-ONE, even when $K_v\beta$2 was also expressed (Figure 11A, B), suggesting that 4-ONE has an all-or-nothing effect on K_v1.4 inactivation since the currents that fully inactivate look similar to K_v1.4 C13S currents. However, since 4-ONE can influence K_v1.4 inactivation but not K_v1.4 C13S inactivation, K_v1.4 C13S was used to test various compounds of interest.

The tau values for K_v1.4 C13S and $K_v\beta$2 are lower relative to the tau values for just K_v1.4 C13S and return to K_v1.4 C13S tau value levels with 4-ONE (Figure 11A, B), suggesting that the function of $K_v\beta$2 in its native NADPH bound state (Figure 5A) when complexed with K_v1.4 is to accelerate A-type inactivation. Aside from 4-ONE, several

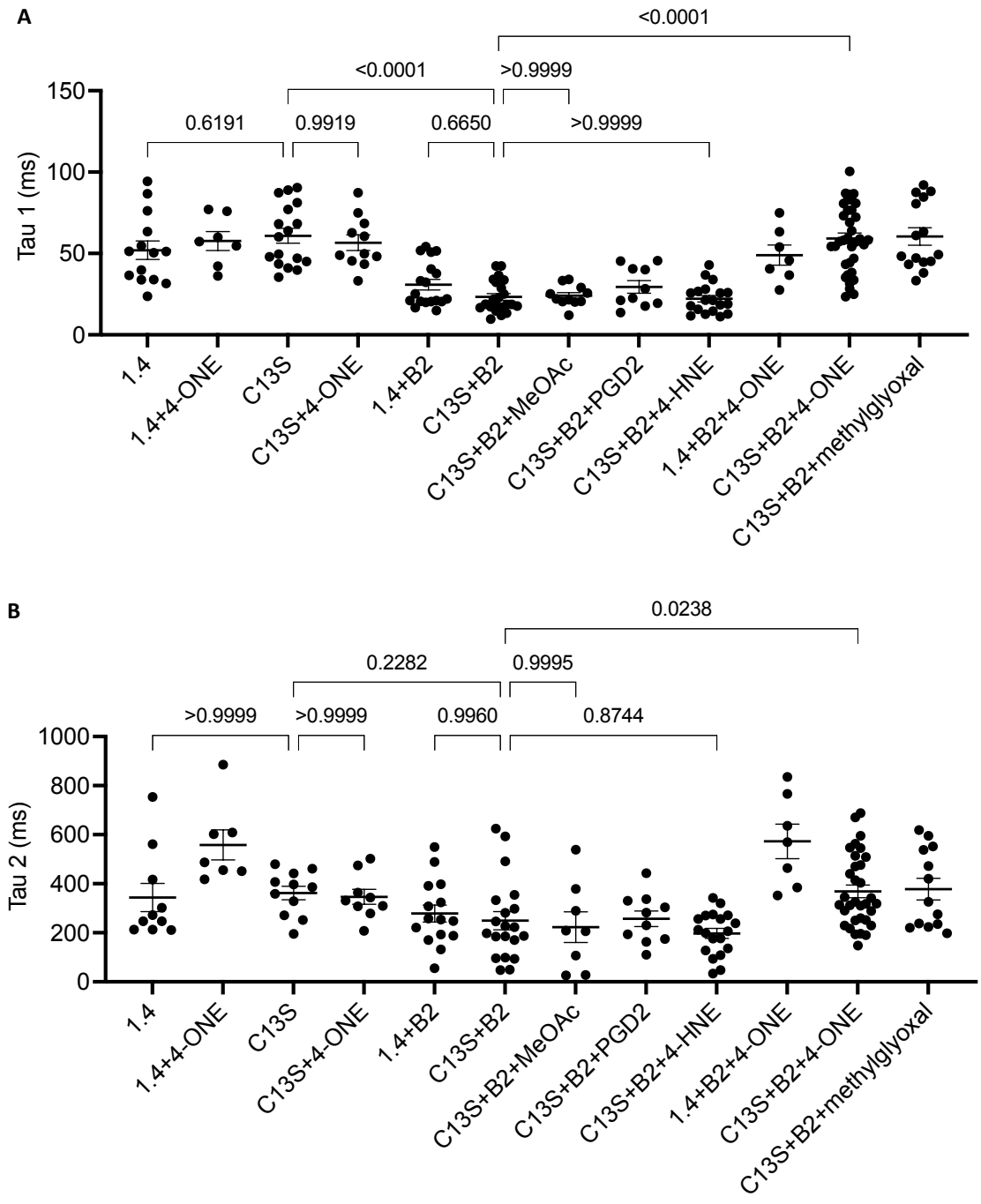


Figure 11. $K_v\beta2$ delays A-type inactivation in a substrate-specific manner

(A) Tau 1 values (shown with both individual values as dots and mean and SEM as horizontal bars), corresponding to τ_{fast}, for various conditions. 1.4 corresponds to $K_v1.4$, C13S corresponds to $K_v1.4$ C13S, B2 corresponds to $K_v\beta2$, and MeOAc corresponds to methyl acetate. For tau values for 1.4+4-ONE and 1.4+B2+4-ONE, currents traces with a partial lack of inactivation were excluded from analysis. Since multiple conditions were being compared, ordinary one-way ANOVAs were used for statistical analysis, specifically Sidak's multiple comparisons test.

(B) Same as (A) but with Tau 2 values, corresponding to τ_{slow}.

other aldehyde- and ketone-containing compounds were tested for their effect on $K_v1.4$ C13S inactivation kinetics through $K_v\beta2$, including 4-HNE, to see whether delayed A-type current inactivation is specific to 4-ONE. Methylglyoxal and prostaglandin D_2 (PGD2)—molecules that have been implicated in sleep but through different mechanisms (Jakubcakova et al., 2013; Nagata and Urade, 2012; Urade and Hayaishi, 2011)—were also tested. PGD2, 4-HNE, and methyl acetate as a vehicle control had no effect on tau values, whereas methylglyoxal significantly increased tau values (Figure 11A, B). Even though PGD2 and 4-HNE contain a ketone and aldehyde functional group, respectively, it has been reported that $K_v\beta2$ exhibits no catalytic activity with PGD2 and 4-HNE, but it does with 4-ONE and methylglyoxal (Tipparaju et al., 2008). 4-HNE is also known to be less reactive than 4-ONE (Lin et al., 2005).

Membrane depolarization leads to decreased inactivation time constants

To test whether voltage changes can accelerate $K_v\beta2$'s cofactor exchange in the context of its role as a biochemical memory sensor, HEK-293 cells expressing $K_v1.4$ C13S and $K_v\beta2$ were incubated in extracellular solution containing methylglyoxal for 1 hour. Cells were then washed three times with normal extracellular solution and voltage clamp recordings were performed. Since methylglyoxal is membrane permeable, it should be able to react with $K_v\beta2$ and oxidize its cofactor to become NADP+. Then if $K_v\beta2$ cofactor exchange is voltage-gated, the NADP+ pool caused by the extracellular methylglyoxal would be exchanged for NADPH following depolarization, which would be reflected in decreased tau values, since $K_v\beta2$ more tightly binds NADPH (the K_d value for $K_v\beta2$ for NADPH is 0.12 uM, whereas it is 0.36 uM for NADP+) (Liu et al., 2001).

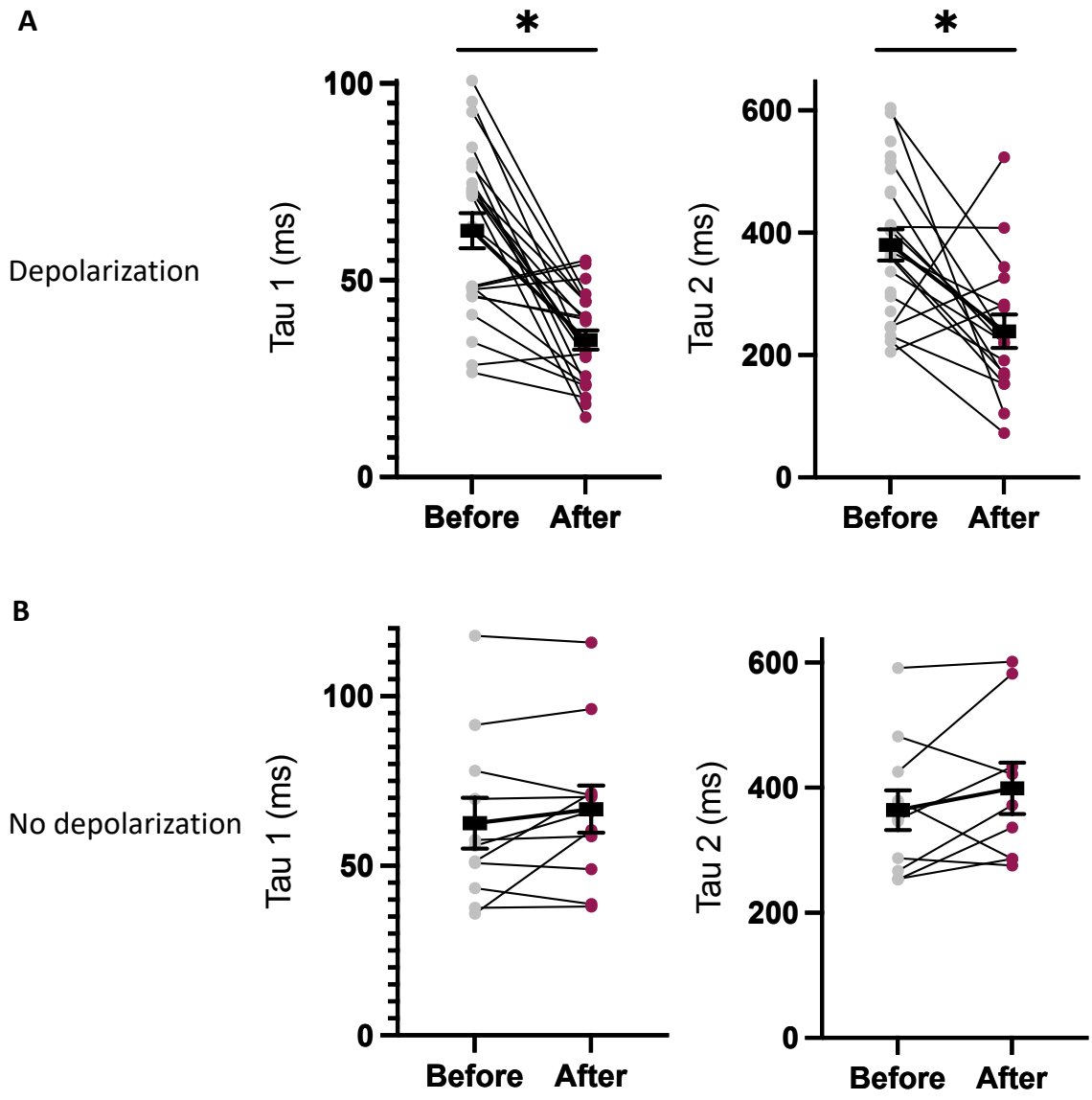


Figure 12. Membrane depolarization leads to decreased inactivation time constants

(A) Tau 1 and 2 values before and after a 20 minute depolarization protocol. Dots represent individual tau values, with grey being before and red being after the respective protocols. Bars with horizontal lines show means with SEM. Since before and after values were analyzed from the same cell following depolarization, paired t-tests were used for statistical analysis ($p<0.0001$ for tau 1, $p=0.0078$ for tau 2)

(B) Tau 1 and 2 values before and after cells were maintained at a holding potential of -80 mV for 20 minutes. Differences were insignificant ($p=0.2008$ for tau 1, $p=0.2420$ for tau 2, paired t-tests).

Indeed, even after the washes, the tau values were comparable to those observed when methylglyoxal was used in the intracellular solution (Figure 11A, B;

Figure 12A, B), suggesting that $K_v\beta2$ can serve as biochemical memory through its probing of the cell's redox state. Following an initial voltage clamp recording to measure tau values, cells underwent a depolarization protocol to rapidly alter the membrane voltage. Tau values significantly decreased following the depolarization protocol (Figure 12A), whereas they slightly increased in the control condition where cells were maintained at a holding potential of -80 mV for the same duration as the depolarization protocol (Figure 12B). In both conditions, the same electrode was used for both the before and after recordings.

Discussion

In the context of sleep regulation, oxidized $K_v\beta$ cofactors delay A-type current inactivation and increase action potential frequency (Kempf et al., 2019). If lipid peroxidation products do indeed serve as the native regulators of $K_v\beta$ subunits, then they should be able to influence A-type current inactivation through $K_v\beta$ subunits, though this has not been demonstrated before.

The work presented in this chapter provides direct evidence that lipid peroxidation breakdown products can delay A-type current inactivation (Figure 11). Interestingly, it appears that the function of $K_v\beta2$ with its natively bound NADPH is to decrease the inactivation time constant of A-type currents, which is then brought back up to tau values observed for $K_v1.4$ only when NADPH becomes oxidized (Figure 11). Thus, when ROS levels increase and generate oxidized byproducts, $K_v\beta2$ registers this change through NADPH being oxidized to become NADP+, thereby slowing A-type current inactivation through $K_v\beta2$'s role as an integrator of oxidative signals. However,

the methods presented here utilized high concentrations of putative substrates in the intracellular solution. To reach more physiologically relevant conclusions about how lipid peroxidation products influence A-type inactivation through $K_v\beta2$, oxidative perturbations to mitochondrial functioning within HEK-293 cells should be used during patching, such as ectopic expression of enzymes involved in regulating oxidative stress and radical scavenging to alter the redox state of the cell (Hill et al., 2018; Kempf et al., 2019). Another possibility to achieve even greater stoichiometric control over substrate delivery is to administer aldehyde or ketone substrates into the Kvβ active site via Halo-tagged fusion Kvβ proteins (Parvez et al., 2016). The relevant substrates bound to the Halo tag will be located near the Kvβ active site and can be released upon UV illumination. Since the number of attached Halo tags can be modified, this experiment would reveal how many catalytic cycles and enzymatic conversions are necessary to modify A-type current.

Since there is no functional difference between expressing only $K_v1.4$ and expressing $K_v1.4$ with $K_v\beta2$ bound to NADP+ in terms of inactivation time constants, there are potential pharmacological implications for molecules that can dissociate $K_v\beta$ subunits—such as cortisone, which has been demonstrated *in vitro* but not *in vivo* (Pan et al., 2008b)—or inhibit them (Alka et al., 2014). By dissociating $K_v\beta$ subunits, A-type currents would be constantly delayed, whereas depending on when $K_v\beta$ subunit activity is inhibited, the cofactor's oxidative state could either be locked into the NADPH or NADP+ state. This would have obvious implications for mammalian sleep once the role of $K_v\beta$ subunits in mammalian sleep is better understood. For flies, more information about the nature of how Hyperkinetic regulates Shaker currents is needed. Does the

presence of Hyperkinetic in its NADPH state also decrease tau values for Shaker, and brings them back up to Shaker only tau values in the presence of oxidizing agents such as lipid peroxidation products? It would be interesting to patch from the dFB in Hk null flies (or from the dFB in fly lines expressing Hk RNAi) to see how the tau values compare to dFB recordings in WT flies to better understand how the presence of Hyperkinetic influences A-type inactivation. Hyperkinetic could then be overexpressed in the dFB in Hk null flies to see what the reintroduction of Hk does to A-type currents. These electrophysiological experiments could also be attempted in a reconstituted system capable of expressing *Drosophila* proteins. If the range of potential tau values is broader for Hyperkinetic and Shaker than it is for $K_v\beta2$ and $K_v1.4$, then pharmacological interventions targeting Hyperkinetic could have a wider range of effects depending on the timing of delivery and function of the modulation.

After lipid peroxidation products arrive and oxidize $K_v\beta$ cofactors to NADP+, a mechanism must exist to allow $K_v\beta$ subunits to release their tightly bound NADP+ cofactors to be replaced with NADPH, for which $K_v\beta2$ has a higher binding affinity (Liu et al., 2001). Previous findings have reported a voltage-dependent regulation of NADPH oxidation, raising the possibility that cofactor turnover may be accelerated by membrane depolarization (Pan et al., 2008a). Indeed, it was found that persistent membrane depolarization decreased tau values, reflecting replacement of NADP+ with NADPH (Figure 12). In the context of $K_v\beta$ subunits being oxidative integrators for *Drosophila* sleep, this would allow Hyperkinetic's pool of oxidized NADP+ cofactors that accumulated throughout the day during dFB electrical silence to be replaced by NADPH during sleep when dFB neurons are electrically active. The action potentials and

corresponding membrane depolarizations that occur in the dFB during sleep would thus reset Hyperkinetic's cofactor pool to NADPH, thereby allowing it to restart the oxidative cycle again in the morning (Figure 1).

In addition to influencing A-type currents through $K_v\beta2$, it was also found that 4-ONE partially prevents the inactivation of $K_v1.4$ currents, thereby demonstrating that lipid peroxidation products can influence A-type inactivation through both alpha and beta subunits (Figure 10). Partial lack of $K_v1.4$ population inactivation has previously been reported during inside-out patches that oxidize the ion channel, but this effect has never been demonstrated through substrates (Ruppersberg et al., 1991). In previous recordings, 4-cyanobenzaldehyde failed to induce this effect, likely because it did not have the same oxidative strength as 4-ONE (Weng et al., 2006). Since a $K_v1.4$ C13S mutation abolishes this effect, it is unlikely that lipid peroxidation products would affect Shaker currents because based on sequence alignment of Shaker and $K_v1.4$, Shaker does not have a conserved cysteine residue in its N-terminal inactivation chain, though a partial lack of Shaker inactivation due to oxidation has not been directly tested.

The work presented here also provides the first evidence for a potential neuroprotective role of $K_v\beta2$ by shielding $K_v1.4$ from 4-ONE (Figure 10E), though a protective role for an aldehyde reductase against ROS-generated lipid peroxidation products has previously been demonstrated in *E. coli* (Pérez et al., 2008). By preventing reactive substrates from reaching alpha subunits, $K_v\beta2$ could protect them from oxidative damage under conditions of high oxidative stress, which has implications for cardiac health and potentially mammalian sleep if a sleep-relevant role for $K_v\beta2$ and $K_v1.4$ is uncovered (Barry et al., 1998; Tur et al., 2017; Guo et al., 2000). To test

whether $K_v\beta2$'s ability to shield $K_v1.4$ from lipid peroxidation products is due to steric effects or catalytic reduction, cells expressing a catalytically dead $K_v\beta2$ subunit, such as a D85N or K118M mutation, alongside $K_v1.4$ should be recorded from in the presence of 4-ONE (Weng et al., 2006). If the effect is solely due to steric hindrance, then a catalytically dead $K_v\beta2$ mutant should have the same effect as a WT $K_v\beta2$, but if the effect is due to catalytic reduction and clearance of lipid peroxidation products, then a catalytically dead $K_v\beta2$ mutant should have no effect. If it is due to some combination of the two, then a catalytically dead $K_v\beta2$ mutant should have a partial effect on preventing $K_v1.4$ inactivation in the presence of 4-ONE.

Results chapter 3: Altering sleep profiles through manipulating Hyperkinetic's cofactor exchange rate

Introduction

As an aldo-keto reductase, Hyperkinetic has an *in vivo* role in redox regulation in flies (Ueda & Wu, 2008). Further work has implicated Hyperkinetic's catalytic activity in coupling mitochondrial ROS sensing in the dFB in the context of sleep regulation to altered Shaker currents, which, similar to $K_v1.4$, is also a potassium ion channel with A-type currents that contribute to membrane repolarization following action potentials (Pimentel et al., 2016; Kempf et al., 2019). Critically, this process was dependent upon Hyperkinetic's intact catalytic activity since a catalytically dead version of Hyperkinetic failed to rescue an insomniac phenotype, whereas a wild type version did (Kempf et al., 2019). Since Hyperkinetic's enzymatic activity plays a crucial role in coupling redox sensing to altered membrane excitability in the context of sleep, the aim of this chapter was to investigate whether sleep profiles can be manipulated solely through altering Hyperkinetic's cofactor exchange rate. This would provide further evidence that Hyperkinetic's role in sleep regulation is through serving as a biochemical integrator of sleep pressure through ROS signaling, whereby increased sleep pressure leads to increased ROS signaling in the dFB, which translates to oxidative conversion of NADPH to NADP+ to serve as a biochemical memory of accumulated sleep pressure (Kempf et al., 2019).

If this were true, then increasing Hyperkinetic's catalytic rate would lead to a less efficient integrator of accumulated sleep pressure, thereby leading to less total sleep.

Previous work has shown that the rate-limiting step for $K_v\beta2$ activity is cofactor exchange (Weng et al., 2006). Since Hyperkinetic has a highly similar conserved core catalytic region as $K_v\beta2$ (Gulbis et al., 1999; Chouinard et al., 1995), this chapter sought to confirm whether cofactor exchange would also be the rate-limiting step for Hyperkinetic. Direct evidence of Hyperkinetic's catalytic activity is also lacking, which this chapter sought to demonstrate. Following confirmation of Hyperkinetic's catalytic capabilities, mutants meant to increase cofactor exchange were designed and tested for their sleep profiles. Previous work on AKR5C3, and aldo-keto reductase in bacteria, identified a mutant that led to a significantly higher NADPH exchange rate (Liu et al., 2014). Importantly, similar to $K_v\beta2$, AKR5C3 has an enclosed NADPH cofactor binding pocket that is altered in the mutant (Gulbis et al., 1999; Liu et al., 2014), suggesting that mutations in amino acids overlying the cofactor binding site may lead to a similar increased turnover rate for Hyperkinetic. As such, amino acids overlying the cofactor binding pocket were targeted in Hyperkinetic, and the effects of these mutants were tested on sleep profiles.

Native genomic Hyperkinetic expression is detectable in the dFB

Though overexpressing Hyperkinetic in the dFB in a Hyperkinetic null background restores sleep to wild-type levels (Kempf et al., 2019), it is not known whether Hyperkinetic is natively expressed in the dFB. To test this, a CRISPR knock-in fly line was generated with an N-terminal FLAG tag on four different Hyperkinetic isoforms in a wild type background to endogenously tag native Hyperkinetic expression (Figure 13A). Western blot analysis from whole fly heads revealed that the CRISPR

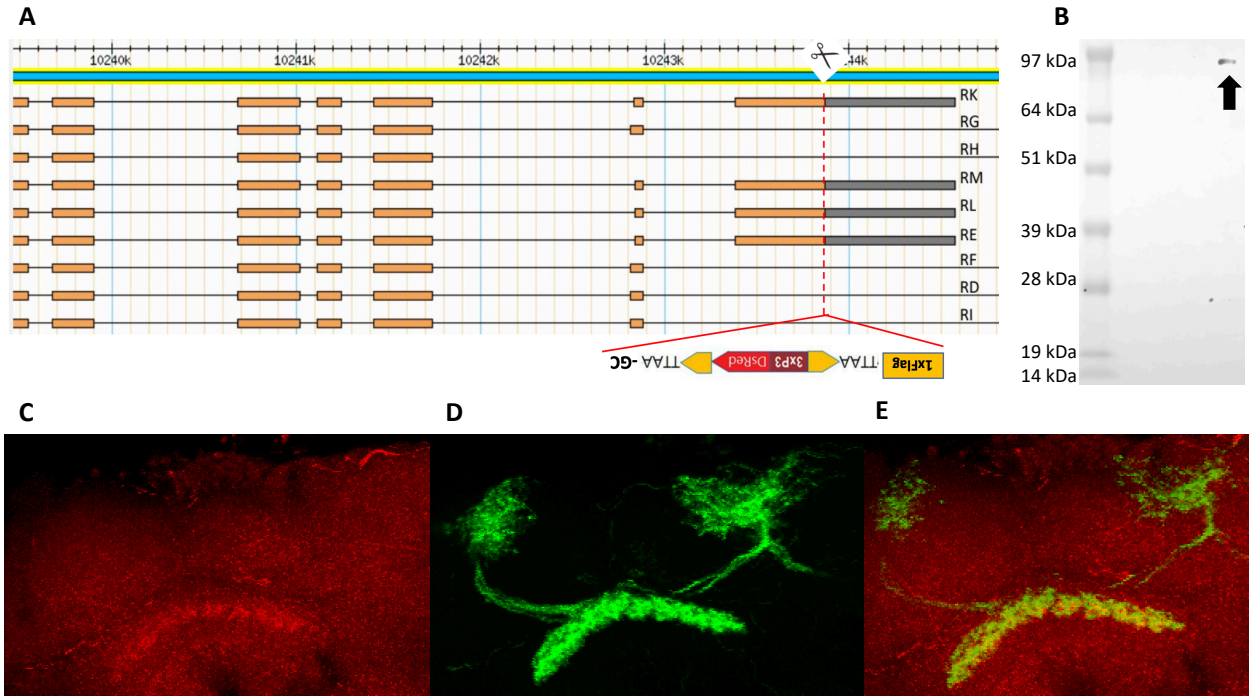


Figure 13. Native genomic Hyperkinetic expression is detectable in the dFB

(A) Schematic for designing a *Drosophila melanogaster* CRISPR knock-in line with an N-terminal FLAG-tagged fusion protein of Hyperkinetic isoforms RE, RK, RL, and RM. The FLAG construct was inserted after the first methionine, and sequences encoding a 4xGGS linker connect the FLAG construct with the gene. 3xP3-DsRed was used as a selection marker to facilitate genetic screening and was excised using PiggyBac transposase.

(B) Western blot of whole fly heads from the CRISPR knock-in line stained with FLAG. Hyperkinetic RM has a molecular weight of ~96 kDa, whereas isoforms RE, RK, and RL all have a molecular weight of ~60 kDa. The FLAG band sits right under the 97 kDa protein ladder.

(C) Homozygous CRISPR knock-in flies were crossed with a *23E10-GAL4 UAS-CD8::GFP* line. Representative confocal image of the brain from a male offspring stained for FLAG (red).

(D) Same as (C) but imaged with 488nm excitation to visualize GFP expression.

(E) Overlay of the images in (C) and (D).

knock-in line expresses a FLAG construct and that Hyperkinetic RM is the most prominently expressed isoform (Figure 13B). Immunofluorescence imaging of brains from the knock-in line concurrently expressing GFP in the dFB through *23E10-GAL4* revealed that Hyperkinetic is prominently expressed in the axons of dFB neurons (Donlea et al., 2018) (Figure 13C-E).

Designing Hyperkinetic mutants for sleep analysis

Previous findings have identified amino acid residues overlying the cofactor binding pocket as potential targets (R192G in AKR5C3) for accelerating aldo-keto reductase enzymatic activity (Liu et al., 2014; Krump et al., 2014; Wang et al., 2014). To that end, amino acid sites in $K_v\beta2$ overlying NADPH were identified as potential targets (Figure 14A, B). Though R192 is not conserved in $K_v\beta2$ or Hyperkinetic, both contain a conserved arginine motif overlying the cofactor binding pocket (Figure 14A, B). Homologous mutation sites in Hyperkinetic that overlie the putative cofactor binding pocket in a predicted structural model were identified via sequence alignment with $K_v\beta2$ based on its bound NADPH cofactor (Figure 14A, B).

Before testing the Hyperkinetic mutants' effect on sleep, the Hyperkinetic null flies were first verified. Compared with Canton-S (CS) control flies, heterozygous Hyperkinetic null flies displayed no significant difference in total sleep, whereas homozygous Hyperkinetic null flies slept significantly less (Figure 14C). The introduction of the *R23E10-GAL4* driver line leads to a further small but significant decrease in total sleep, presumably due to a genetic background effect (Figure 14C).

Increased Hyperkinetic cofactor exchange rate leads to partial sleep rescue

Expression of N-terminally His-tagged Hyperkinetic constructs purified from bacteria was confirmed via Western blot (Figure 15A). In a multiple turnover assay, different concentrations of 9,10-Phenanthrenequinone, a substrate with which $K_v\beta2$ demonstrates high specific activity (Tipparaju et al., 2008), were incubated with a constant amount of purified Hyperkinetic and excess NADPH. Absorbance at 340 nm

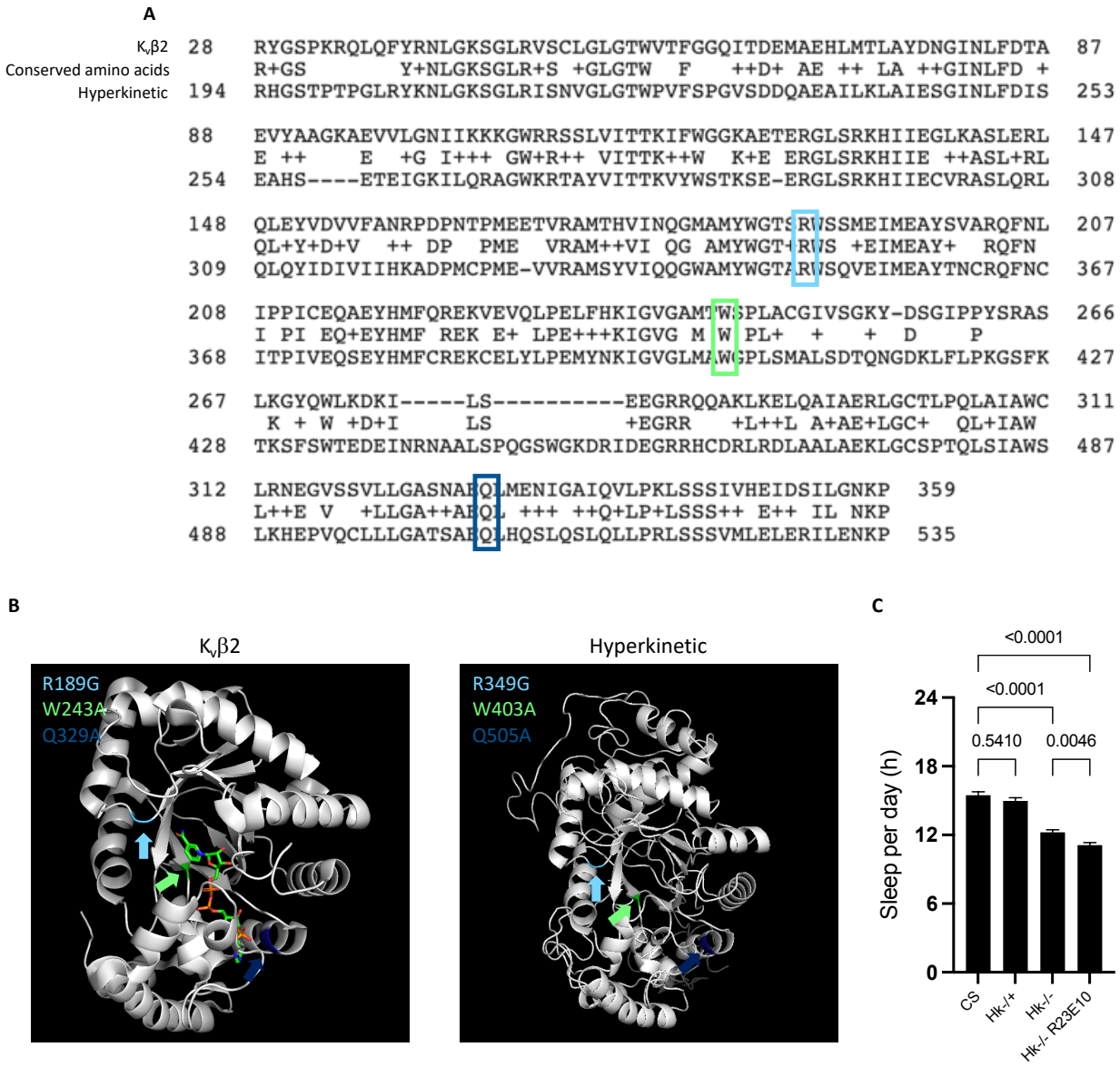


Figure 14. Identifying Hyperkinetic mutants for sleep analysis

(A) Protein BLAST results from NCBI demonstrating highly conserved core regions between $K_v\beta2$ and Hyperkinetic. Conserved mutants of interest are highlighted in the colored boxes, with the colors corresponding to the mutants used in Figure 12.

(B) (Left) Ribbon structure of $K_v\beta2$ with the co-purified NADPH cofactor in the middle. (Right) Predicted ribbon structure of Hyperkinetic with an empty cofactor binding pocket presented from the same angle as $K_v\beta2$. $K_v\beta$ amino acid mutation sites of interest are highlighted with arrows pointing to the specific site with the color coordination shown in the top left-hand corner.

(C) Sleep profiles of various control fly lines (n>32 for all conditions over n>3 independent experiments) demonstrate that a Hk-/- background, but not a heterozygous background, leads to decreased sleep compared to CS flies. Tukey's multiple comparisons test was used for statistical analysis.

was monitored to measure the steady-state NADPH turnover rate (Weng et al., 2006; Tipparaju et al., 2008). Similar to $K_v\beta2$, the steady-state turnover rate for Hyperkinetic saturates with increasing substrate concentration (Figure 15B), consistent with the observation for $K_v\beta2$ that cofactor exchange is the rate limiting step (Weng et al., 2006). This also provides direct evidence that Hyperkinetic is a functional aldo-keto reductase. Compared to Hyperkinetic WT, the three mutants have similar saturation curves but higher steady-state NADPH turnover rates (Figure 15B, C).

Interestingly, when these Hyperkinetic constructs were ectopically overexpressed in the dFB in a homozygous Hyperkinetic null background, the three mutants displayed a partial sleep rescue that inversely correlated with their steady-state NADPH turnover rate when compared to the WT control (Figure 15D). Furthermore, consistent with Hyperkinetic's role as a ROS sensor that helps drive flies to sleep, expression of Hyperkinetic in the dFB increases the number of sleep bouts but does not increase sleep bout length (Figure 15E, F). This effect is statistically significant for Hyperkinetic WT, R349G, and W403A, but not for Q505A, though there is a trend towards an increase in the number of sleep bouts per day (Figure 15E, F).

Discussion

If Hyperkinetic serves as an integrator of accumulating ROS signals during wake to drive the fly to sleep, then its capacity as an integrator should be able to be modulated through manipulating its enzymatic activity. As an aldo-keto reductase, its rate limiting step is cofactor exchange (Figure 5B) (Weng et al., 2006). As such, targeting amino acid residues involved in cofactor binding and release to accelerate

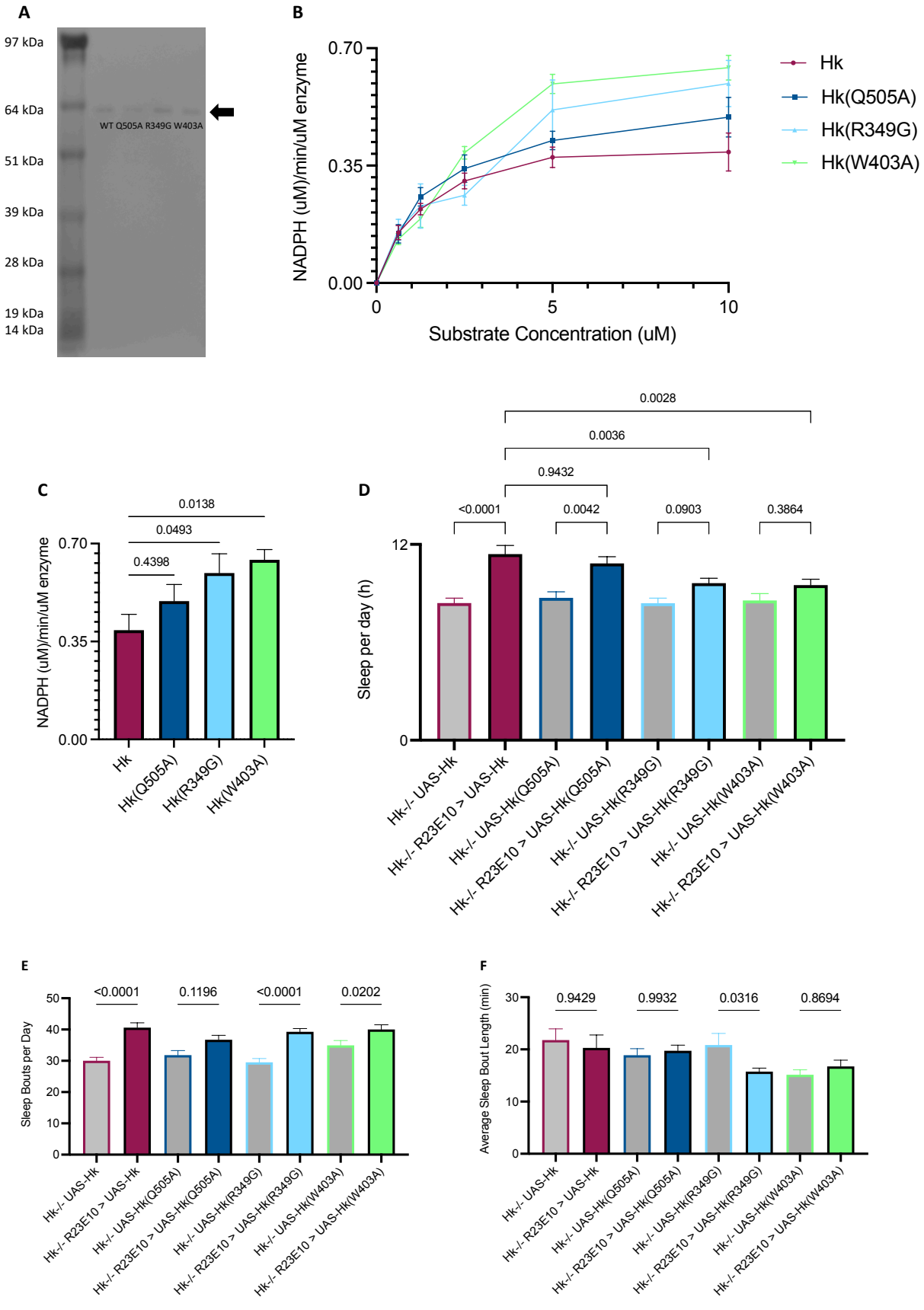

A
97 kDa
64 kDa
51 kDa
39 kDa
28 kDa
19 kDa
14 kDa
WT Q505A R349G W403A
B
NADPH (uM)/min/uM enzyme
0.70
0.35
0.00
0
5
10
Substrate Concentration (uM)
Hk
Hk(Q505A)
Hk(R349G)
Hk(W403A)
C
NADPH (uM)/min/uM enzyme
0.0138
0.0493
0.4398
Hk
Hk(Q505A)
Hk(R349G)
Hk(W403A)
D
Sleep per day (h)
0.0028
0.0036
0.9432
<0.0001
0.0042
0.0903
0.3864
Hk-/- UAS-Hk
Hk-/- R23E10 > UAS-Hk
Hk-/- UAS-Hk(Q505A)
Hk-/- R23E10 > UAS-Hk(Q505A)
Hk-/- UAS-Hk(R349G)
Hk-/- R23E10 > UAS-Hk(R349G)
Hk-/- UAS-Hk(W403A)
Hk-/- R23E10 > UAS-Hk(W403A)
E
Sleep Bouts per Day
<0.0001
0.1196
<0.0001
0.0202
F
Average Sleep Bout Length (min)
0.9429
0.9932
0.0316
0.8694

Figure 15. Increased Hyperkinetic cofactor exchange rate leads to partial sleep rescue

(A) Western blot of the concentrated Hyperkinetic proteins purified from bacteria stained with an anti-His antibody. Hyperkinetic WT's monomeric weight is ~62.2 kDa, and the bands sit below the protein ladder mark for ~64 kDa.
(B) Steady-state NADPH turnover rates plotted versus substrate concentration for various Hyperkinetic constructs (n=6 for each substrate concentration for all constructs).
(C) Steady-state NADPH turnover rates from (B) plotted for 10 uM of substrate. Dunnett's multiple comparisons test was used for statistical analysis.
(D) Sleep profiles for the various Hyperkinetic constructs (n>32 for all conditions spread over n>3 independent replicates). Sidak's multiple comparisons test was used.
(E) Number of sleep bouts per day for the various Hyperkinetic constructs. All data were analyzed from the same data set collected for (D). Sidak's multiple comparisons test was used.
(F) Average sleep bout length for the various Hyperkinetic constructs. All data were analyzed from the same data set collected for (D). Sidak's multiple comparisons test was used.

cofactor exchange should compromise its ability as an integrator. Thus when ROS signals arrive and convert NADPH to NADP+, bound NADP+ would be replaced by NADPH at a faster rate than it would for WT Hyperkinetic, thereby resulting in less total sleep.

Indeed, there was an inverse correlation between the steady-state NADPH turnover rate and how much sleep was restored for the Hyperkinetic mutants (Figure 15). Future work will address whether the mammalian mutant homologs couple to $K_v\alpha$ subunits and modulate A-type currents to ensure proper expression and functioning. Furthermore, consistent with the idea of Hyperkinetic being an integrator in the dFB that drives the fly to sleep, native expression of Hyperkinetic in the dFB was confirmed (Figure 13C-E), and Hyperkinetic expression in the dFB in a Hk null background increased the number of sleep bouts without increasing sleep bout duration (Figure 15E, F). The converse effect, whereby slowing down cofactor exchange should result in increased sleep, however, has not yet been tested.

Previous work has reported that W243A and R189M mutations in $K_v\beta2$ do not significantly alter K_d for NADPH compared to wild type $K_v\beta2$ (Liu et al., 2001). Given that

R189M differs from R189G, this is not a direct comparison. However, for W243A, the K_d measured was not performed in the presence of substrates (Liu et al., 2001), which could affect cofactor turnover rate for an aldo-keto reductase that reduces a broad range of substrates (Tipparaju et al., 2008). As such, K_d and steady-state NADPH turnover rate may not be directly comparable with each other.

These results are the first to directly demonstrate Hyperkinetic's catalytic activity as an enzyme (Figure 15B, C) and its native expression in the dFB (Figure 13C-E). Although much is known about mammalian $K_v\beta$ subunits, much less is known about Hyperkinetic, especially since nine different isoforms exist. For instance, it is not known which isoform(s) is involved in sleep regulation in the dFB, nor is it known how or if different isoforms regulate Shaker currents. In order to add to the growing body of literature for Hyperkinetic and its role in *Drosophila* neurons, more biochemical, structural, and electrophysiological data are needed, particularly for the various isoforms. Different Hyperkinetic isoforms could be purified from Sf9 cells and used for structural and biochemical studies to give more insight into its catalytic activity and regulation, and the roles for different isoforms in sleep regulation could be tested, though this may be difficult given the large number of shared exons between isoforms. This insight could then be combined with electrophysiology data for the different Hyperkinetic isoforms to create a more comprehensive picture of how $K_v\beta$ subunits contribute to sleep regulation in *Drosophila*.

Discussion and Future Directions

The data presented in this thesis support the notion that $K_v\beta$ subunits can act as voltage-sensitive enzymatic integrators of lipid peroxidation products to help influence sleep through modulating A-type currents. Key findings and conclusions were discussed in the broader context of $K_v\beta$ subunit regulation of sleep in the corresponding chapters' discussion sections. However, several potentially confounding factors and additional considerations must be considered given the data presented in this thesis. Several future experiments and areas of inquiry are also presented in this section.

POVPC reduction and binding

The results from chapter 1 suggest that the purified $K_v\beta2$ was a functional enzyme, as demonstrated through reduction of POVPC (Figure 5). However, no control experiment was done for this. It is possible that a contaminant in the purified protein catalyzed the reduction instead, though this is unlikely given that proteomics of the eluted protein sample confirmed its purity. Additionally, no other proteins were observed in the highly sensitive native MS (Figure 6), and no other bands appeared on the Coomassie gel (Figure 4), though more protein should have been loaded to confirm this. However, to conclusively rule out the possibility that a contaminant present at undetectable levels reduced POVPC, a catalytically dead mutant of $K_v\beta2$ with the same FLAG tag and purified in an identical manner should have been used. Several catalytically dead $K_v\beta2$ mutants have demonstrated (Y90F, K118M, D85N) (Tipparaju et al., 2008; Weng et al., 2006). If the catalytically dead mutants are able to still reduce POVPC, and the possibility of contaminants can somehow be ruled out, then this may

indicate that the assay used in this thesis to demonstrate POVPC reduction may not be suitable and alternative methods of demonstrating catalytic activity should be pursued instead.

It is interesting to note that POVPC binding to $K_v\beta2$ was not observed (Figure 8). Perhaps this is because $K_v\beta2$ did not actually reduce POVPC, which would explain why the binding was not observed. However, if it can be assumed that $K_v\beta2$ successfully reduced POVPC, perhaps the incubation conditions to test POVPC were not ideal to capture binding via MS. The incubation time used for binding studies, 5 minutes, was significantly shorter than the incubation time used for reduction experiments, 3 hours. To further investigate whether POVPC can stably bind to $K_v\beta2$ for MS detection, incubation times should be increased. It is also possible that POVPC, and other lipid peroxidation products, are labile, and their instability leads to transient binding that cannot be detected by MS methods.

Endogenous expression of K_v subunits in HEK-293 cells

Furthermore, the results from Chapter 1 and 2 use HEK-293 cells to ectopically overexpress K_v subunits. Using RT-PCR and electrophysiology data, it has been shown that HEK-293 natively express several K_v ion channels (Jiang et al., 2002). RT-PCR was also able to amplify transcripts for $K_v\beta2$ (Jiang et al., 2002). These findings potentially complicate interpretation of the results presented.

Although Jiang et al. (2002) provided electrophysiological evidence of native K_v ion channel expression in HEK-293 cells, the untransfected HEK-293 cells used in this thesis did not exhibit any evoked currents (Figure 4G) under the same voltage clamp

protocol that was used to study $K_v1.4$ (Figure 11), suggesting that perhaps the cells used in this thesis do not have sufficient, or perhaps any, expression of K_v ion channels detectable by voltage clamp. Furthermore, when $K_v\beta2$ was ectopically overexpressed, it was found to be spread out through the cytoplasm (Figure 4D). If the cells used in this thesis natively express K_v ion channels, there should be an enrichment of $K_v\beta2$ signal at the plasma membrane, but this was not observed.

Furthermore, it is important to note that while Jiang et al. (2002) looked at transcript amplification for $K_v\beta2$, they did not analyze $K_v\beta2$ protein expression. There was no detectable antibody signal for untransfected HEK-293 cells stained with an anti-$K_v\beta2$ antibody. Furthermore, the calculated mass for the purified $K_v\beta2$ corresponds to the theoretical octameric mass of the $K_v\beta2$-FLAG construct used (327,280.40 Da), ruling out the possibility of native $K_v\beta2$ incorporation since native full-length $K_v\beta2$ has a different mass. Proteomics analysis confirmed this since the first 35 amino acids of $K_v\beta2$ were removed to prevent aggregation, and no peptides corresponding to the first 35 amino acids were found in the proteomics search. Lastly, the Coomassie gel, though underloaded, only had one visible band (Figure 4I), whereas two would be expected if native $K_v\beta2$ was incorporated. To confirm the lack of native $K_v\beta2$ in the HEK-293 cells used in this thesis, RT-PCR and proteomics analysis of the cells could be performed.

Given this, however, it is not fully possible to rule out the possibility that when HEK-293 cells were transiently transfected with $K_v1.4$ C13S, these ion channels complexed with native $K_v\beta2$, though this scenario is unlikely given no native $K_v\beta2$ expression was detectable via several methods. Furthermore, when $K_v\beta2$ was transiently co-expressed with $K_v1.4$ C13S, tau values decreased (Figure 11), suggesting

that many if not all of the K_v1.4 C13S channels were not bound to $K_v\beta$2. Thus, even if traces amount of native $K_v\beta$2 were bound, they would unlikely have any effects on channel modulation. To confirm that no native $K_v\beta$2 was bound to K_v1.4 C13S, a FLAG-tagged version should have been expressed by itself and purified. Subsequent immunostaining and proteomics analysis would have then been able to probe whether any detectable $K_v\beta$2 was present. However, if it is assumed that K_v1.4 C13S complexed with native $K_v\beta$2, there are three primary scenarios to consider in this case: the K_v1.4 C13S-bound, native $K_v\beta$2 is bound to a mixture of NADP+/NADPH, or it is predominantly bound to either NADP+ or NADPH.

The most likely of these three scenarios is that the potential native $K_v\beta$2 would be bound to NADPH given $K_v\beta$2's preferential binding for NADPH over NADP+ (Liu et al., 2001). Further evidence to support this is that purified $K_v\beta$2, whether from HEK-293 cells (Figure 5A) or from bacteria (Weng et al., 2006; Tipparaju et al., 2008), is found to be bound to NADPH. Bound NADP+ has only been observed in crystallized structures (Gulbis et al., 1999; Long et al., 2005), presumably from the lengthy crystallization process. If native $K_v\beta$2 was bound to NADP+/NADPH or predominantly NADPH, then addition of 4-ONE would have increased tau values, which was not observed (Figure 11).

If transiently expressed K_v1.4 C13S did complex with native $K_v\beta$2 bound to predominantly NADP+, then including substrates with alcohol functional groups in the intracellular solution when performing voltage clamps would decrease tau values since the substrates would reduce the bound cofactors to NADPH. Performing this study

would rule out this final possibility, but such experiments were not performed in this thesis.

Although this final possibility could not be ruled out, it does not significantly alter interpretation of the results presented here since any trace amounts of native $K_v\beta2$ do would not have a noticeable effect in electrophysiological recordings and since $K_v\beta2$ bound to NADP+ would not react with 4-ONE or other molecules with aldehydes or ketones.

4-ONE leads to a partial lack of inactivation for $K_v1.4$

Though 4-ONE alters $K_v1.4$ inactivation profiles as observed through voltage clamp recordings, inactivation still occurs but to a smaller extent (Figure 10). As such, on the channel population level within the membrane patch being recorded from, there is a substantial partial lack of inactivation. Perhaps in the presence of 4-ONE, all $K_v1.4$ channels underwent oxidation at the C13 residue, and the subsequent disulfide bridges that formed to prevent chain inactivation of the pore were not sufficient enough to completely prevent the chains from occluding the pore (Ruppersberg et al., 1991), thereby leading to the observed partial lack of inactivation. Another possibility is that some $K_v1.4$ channels were completely unable to inactivate in the presence of 4-ONE where others were, thereby also leading to a partial lack of inactivation on the channel population level. It was not possible to achieve single channel resolution to observe why a partial lack of inactivation occurred, but future experiments that can record from single channels would be able to achieve better insight into how oxidation affects $K_v1.4$ inactivation. Another future experiment that would elucidate how cysteine oxidation in

K_v1.4's N-terminal inactivation chain affects pore occlusion would be to resolve the structures of purified K_v1.4 with and without C13 oxidation.

As mentioned in the discussion in Chapter 2, different $K_v\beta$2 mutants could be used with K_v1.4 to better understand how $K_v\beta$2 prevents this partial lack of inactivation. Similar studies could also experiment with different exposure times and substrate concentrations. Perhaps the all or nothing effect of 4-ONE on K_v1.4 inactivation (Figure 11) was due to insufficient time for 4-ONE to reach the K_v1.4 channels. However, it should be noted that in the presence of $K_v\beta$2, 4-ONE still lead to a comparable increase in tau values for both K_v1.4 and K_v1.4 C13S (Figure 11), suggesting that even if 4-ONE was not reaching K_v1.4 in time, it had sufficient time to reach and react with $K_v\beta$2. Nonetheless, future experiments could expose K_v1.4 to different lengths of 4-ONE incubation before performing voltage clamp recordings to see if exposure duration affects channel inactivation. If this were the case, longer exposure times to increase the probability of channel oxidation would lead to more pronounced effects on channel inactivation.

Similarly, different concentrations of 4-ONE, and other oxidative substrates, could be tested to confirm if likelihood of oxidation affects inactivation profiles. The concentration of 4-ONE (100 uM) used throughout this thesis is significantly higher than 4-ONE concentrations found endogenously in cells, which is estimated to be in the high pico-low micro molar range, though this has not been conclusively studied (Esterbauer et al., 1991).

Voltage-dependent cofactor exchange

$K_v\beta2$ tightly binds its cofactor, at least *in vitro* (Gulbis et al., 1999), which raises questions of how membrane depolarization can accelerate cofactor turnover (Figure 12), especially since the experiments done in Chapter 2 required only 20 minutes of depolarization to see significant effects. These short time scales rule out any effects due to differential gene expression. Further contributing to this mystery is that $K_v\beta$ subunits bind to K_v ion channels through a T1 domain and are thus not bound to the plasma membrane (Gulbis et al., 2000). This spatial separation cause by the T1 domain makes it even more implausible that voltage changes at the plasma membrane can cause significant changes to $K_v\beta$ subunit activity.

A simple explanation is that $K_v\beta2$ does not bind as tightly to its cofactor *in vivo*, though this has not been directly studied. It may also be possible that extensive conformational changes in $K_v\alpha$ subunits that occur in the transmembrane region due to their voltage sensitivity in the presence of membrane depolarization lead to conformational changes in their T1 domains as well that are then subsequently transduced to the $K_v\beta$ subunits. A series of mutational screens in $K_v\alpha$ could identify regions and residues that contribute to this potential transduction of conformational changes, though it may be difficult to disentangle mutated regions impairing transduction from affecting proper subunit binding, folding, expression, and/or voltage sensitivity.

Another set of experiments to test whether $K_v\beta$ subunits themselves can somehow sense the voltage changes would be tethering $K_v\beta$ subunits to the plasma membrane without expressing $K_v\alpha$ subunits. The $K_v\beta$ subunits would need to be tethered at a distance comparable to the size of the T1 domain (Long et al., 2005). The

membranes could then be depolarized, and the $K_v\beta$ subunits could be purified to examine their cofactor oxidation state and compared to a control condition in which the membranes were not depolarized. If $K_v\beta$ subunits do indeed have a voltage sensitivity mechanism, similar mutational screens could try to identify the responsible regions, though this may also prove difficult.

Before embarking on these proposed experiments, to make the voltage sensitivity data in Chapter 2 more convincing, the following ideal experiment should be conducted. Cells expressing $K_v1.4$ C13s with $K_v\beta2$ should be recorded from to achieve a baseline recording. 4-ONE should be applied and then thoroughly washed away, and the same cell should be recorded from again using the same electrode to observe an increase in tau values. Following this, a depolarization protocol should be applied, after which the cell should be recorded from again to see if the tau values decrease. Finally, 4-ONE should be applied again to see if tau values increase again. This experiment, if successful, would provide more conclusive evidence that membrane depolarization leads to cofactor exchange that can subsequently be modified again through substrate oxidation.

Differential Hyperkinetic expression in the dFB

Through using a CRISPR knock-in line to label four Hyperkinetic isoforms with a FLAG tag in a fly line that endogenously expresses Hyperkinetic, it was found that FLAG signals were only detectable in the axons of the dFB (Figure 13 C-E). There are several possibilities as to why this signal was only detectable in dFB axons. Previous studies have shown that $K_v\beta$ subunits led to axonal targeting of $K_v1.2$ in cultured

hippocampal neurons, which is similar to its expression pattern in brain neurons (Campomanes et al., 2002; Lai & Jan, 2006). Thus, the simplest explanation is that a similar phenomenon is occurring with Hyperkinetic and Shaker. To confirm this, similar experiments in which a CRISPR knock-in line tags Shaker for immunofluorescent visualization should be conducted to test whether the signal is also localized to dFB axons since Shaker expression should overlap with Hyperkinetic expression. It would also be interesting to try this in a Hyperkinetic null background to see whether the expression pattern for Shaker changes in the absence of Hyperkinetic.

It is possible that Hyperkinetic is natively expressed in dFB dendrites and cell bodies, but that expression levels are lower than in the axons and thus not detectable by immunofluorescence imaging. Another possibility is that dFB projection axons have a significantly higher density since they have a communal projection area within the central complex (Donlea et al., 2011; Hulse et al., 2021), which would lead to enhanced immunofluorescence signals compared to the dendrites and cell bodies, which occupy different regions and have minimal overlap (Donlea et al., 2018; Hulse et al., 2021).

It could also be that since only four of the nine Hyperkinetic isoforms were labeled, not all the Hyperkinetic proteins in the dFB were properly imaged. Transcriptomic analysis of dFB neurons to see which Hyperkinetic isoforms have mRNA transcripts would provide better insight, though robust transcriptomic data for the dFB may be difficult given the small number of dFB neurons per brain (Donlea et al., 2011; Hulse et al., 2021). Future experiments could try individually tagging each Hyperkinetic isoform and visualizing their cellular localization to confirm where Hyperkinetic is natively expressed.

Hyperkinetic mutants differentially rescue an insomniac phenotype

It was found that three Hyperkinetic mutants (Q505A, R349G, and W403A) partially rescue sleep compared to wild type Hyperkinetic in a Hyperkinetic null background, though the effect for Hyperkinetic Q505A was not significant compared to wild type Hyperkinetic, but there was a trend towards less sleep (Figure 15D). It should be noted that purified Hyperkinetic Q505A from bacteria did not show a statistically significant increase in steady-state NADPH turnover rate compared to wild type Hyperkinetic, though there was also a trend towards a higher turnover rate (Figure 15C).

One potentially confounding variable for this analysis is that expressing one copy of the *R23E10-GAL4* driver line in a Hyperkinetic null background had a significant effect on sleep (Figure 14C). This effect would be concerning if it led to an increase in sleep since restoring Hyperkinetic expression in the dFB in a Hyperkinetic null background rescues sleep (Kempf et al., 2019), but since it led to a further decrease in sleep on top of the insomniac phenotype of Hyperkinetic null flies, any sleep rescue effects achieved by ectopically overexpressing different Hyperkinetic constructs can be attributed to the overexpression of Hyperkinetic. Furthermore, to control for this potential genomic interaction, genetic backgrounds were controlled for such that the control flies expressed their respective UAS-Hk constructs in a Hyperkinetic null background, and experimental flies all expressed one copy of *R23E10-GAL4* driving UAS-Hk constructs of interest in a Hyperkinetic null background. Since the only difference between these

groups was the Hyperkinetic construct used, any sleep differences observed can be attributed to the unique properties of the Hyperkinetic construct used.

The *R23E10-GAL4* driver line was not crossed into control lines (CS, Hk+/-) since these lines were not used to overexpress Hyperkinetic constructs. The driver line was only crossed into a homozygous Hyperkinetic null background since only the homozygous condition displayed a hyperkinetic phenotype reflected in decreased sleep (Figure 14C).

To accommodate for this potential genetic background effects, however, further statistical analyses were done to compare the overexpression of Hyperkinetic constructs directly to the condition in which Hyperkinetic wild type was overexpressed (Figure 15D). Similar results were found, whereby Q505A did not have a significant decrease in sleep relative to wild type, though there was a downward trend, whereas R349G and W403A did. Interestingly, in both $K_v\beta2$ and the predicted structure of Hyperkinetic, the conserved arginine (R189G for $K_v\beta2$ and R349G for Hyperkinetic) and tryptophan (W243A for $K_v\beta2$ and W403A for Hyperkinetic) mutation sites are located near the nicotinamide region of the bound NADPH, whereas the glutamine (Q329A for $K_v\beta2$ and Q505A for Hyperkinetic) residue is located near the adenine end of NADPH. Perhaps $K_v\beta2$ mutations in the cofactor binding pocket near the nicotinamide region of NADPH lead to accelerated cofactor release compared to mutations in the adenine end. To confirm this however, further mutational screens need to be done on $K_v\beta2$ to test steady-state NADPH turnover rates for various mutations along the NADPH binding pocket.

Future studies could also investigate whether mutating residues in the cofactor binding pocket to further enclose the NADPH cofactor would lead to slower cofactor exchange, and if so, whether these mutations would lead to the converse effect of increased total sleep. However, it may be difficult to differentiate between slower cofactor exchange and misfolded or unfunctional enzymes.

Although the results presented in this thesis provide novel insight into the nature of $K_v\beta$ subunit regulation of sleep, there are still many unanswered questions and mysteries regarding sleep, as discussed throughout the introduction and various discussion sections in this thesis. The lingering complexities reflect the complex nature of sleep itself, and will require significant devoted research efforts over the upcoming decades to gain a more thorough and deeper understanding regarding the vast mysteries of sleep across the animal kingdom.

References

Alka, K., Dolly, J. O., Ryan, B. J. & Henehan G. T. M. (2014). New inhibitors of the Kvβ2 subunit from mammalian Kv1 potassium channels. *Int J Biochem Cell Biol., 55*, 35-39.

Allada, R., Emery, P., Takahashi, J. S. & Rosbash, M. (2001). Stopping time: the genetics of fly and mouse circadian clocks. *Annu Rev Neurosci*, *24*, 1091–1119.

Anafi, R. C., Kayser, M. S. & Raizen, D. M. (2019). Exploring phylogeny to find the function of sleep. *Nat Rev Neurosci*, *20*, 109-116.

Artiushin, G. & Sehgal, A. (2017). The Drosophila circuitry of sleep-wake regulation. *Curr Opin Neurobiol*, *44*, 243-250.

Balaban, R. S., Nemoto, S., & Finkel, T. (2005). Mitochondria, oxidants, and aging. *Cell*, *120*, 483–495.

Barry, D. M., Xu, H., Schuessler, R. B. & Nerbonne, J. M. (1998). Functional knockout of the transient outward current, long-QT syndrome, and cardiac remodeling in mice expressing a dominant-negative Kv4 alpha subunit. *Circ Res.*, *83*, 560-567.

Barski, O. A., Tipparaju, S. M., & Bhatnagar, A. (2008). The aldo-keto reductase superfamily and its role in drug metabolism and detoxification. *Drug metabolism reviews*, *40*, 553–624.

Borbély, A. (2022). The two-process model of sleep regulation: Beginnings and outlook. *J Sleep Res*, *e13598*.

Borbély, A. A. (1982). A two process model of sleep regulation. *Hum Neurobiol*, *1*, 195–204.

Bushey, D., Huber, R., Tononi, G. & Cirelli, C. (2007). *Drosophila Hyperkinetic* mutants have reduced sleep and impaired memory. *J Neurosci*, *27*, 5384-5393.

Campomanes, C. R., Carroll, K. I., Manganas, L. N., Hershberger, M. E., Gong, B., Antonucci, D. E., Rhodes, K. J. & Trimmer, J. S. (2002). Kv beta subunit oxidoreductase activity and Kv1 potassium channel trafficking. *J Biol Chem*, *277*, 8298-8305.

Cavanaugh, D. J., Geratowski, J. D., Wooltorton, J. R., Spaethling, J. M., Hector, C. E., Zheng, X., Johnson, E. C., Eberwine, J. H. & Sehgal, A. Identification of a circadian output circuit for rest: activity rhythms in Drosophila. *Cell*, *157*, 689-701.

Chouinard, S. W., Wilson, G. F., Schlimgen, A. K. & Ganetzky, B. (1995). A potassium channel β subunit related to the aldo-keto reductase superfamily is encoded by the *Drosophila* Hyperkinetic locus. *Proc Natl Acad Sci USA*, *92*, 6763-6767.

Cirelli, C., Bushey, D., Hill, S., Huber, R., Kreber, R., Ganetzky, B. & Tononi, G. (2005). Reduced sleep in *Drosophila Shaker* mutants. *Nature*, *434*, 1087-1092.

Coetzee, W. A., Amarillo, Y., Chiu, J., Chow, A., Lau, D., McCormack, T., Moreno, H., Nadal, M. S., Ozaita, A., Pountney, D., Saganich, M., Vega-Saenz de Miera, E. & Rudy, B. (1999). Molecular diversity of K+ channels. *Annals of the New York Academy of Sciences*, *868*, 233–285.

Connor, J. A. & Stevens, C. F. (1971). Prediction of repetitive firing behaviour from voltage clamp data on an isolated neurone soma. *J Physiol*, *213*, 31-53.

Crane, B. R. & Young, M. W. (2014). Interactive features of proteins composing eukaryotic circadian clocks. *Annu. Rev. Biochem., 83*, 191–219.

Czapski, G. A., Czubowicz, K., Strosznajder, J. B., & Strosznajder, R. P. (2016). The Lipoxygenases: Their Regulation and Implication in Alzheimer's Disease. *Neurochemical research*, *41*, 243–257.

Delventhal, R., O'Connor, R. M., Pantalia, M. M., Ulgherait, M., Kim, H. X., Basturk, M. K., Canman, J. C. & Shirasu-Hiza, M. (2019). Dissection of central clock function in *Drosophila* through cell-specific CRISPR-mediated clock gene disruption. *eLife*, *8*, e48308.

Donlea, J. M., Pimentel, D. & Miesenböck, G. (2014). Neuronal machinery of sleep homeostasis in Drosophila. *Neuron*, *81*, 860–872.

Donlea, J. M., Pimentel, D., Talbot, C. B., Kempf, A., Omoto, J. J., Hartenstein, V. & Miesenböck, G. (2018). Recurrent circuitry for balancing sleep need and sleep. *Neuron*, *97*, 378–389.

Donlea, J. M., Thimgan, M. S., Suzuki, Y., Gottschalk, L. & Shaw, P. J. (2011). Inducing sleep by remote control facilitates memory consolidation in Drosophila. *Science*, *332*, 1571-1576.

Douglad, C. L., Vyazovskiy, V., Southard, T., Chiu, S., Messing, A., Tononi, G. & Cirelli, C. (2007). Sleep in *Kcna2* knockout mice. *BMC Biology*, *5*:42.

Doyle, D. A., Morais, J. C., Pfuetzner, R. A., Kuo, A., Gulbis, J. M., Cohen, S. L., Chait, B. T. & MacKinnon, R. (1998). The structure of the potassium channel: molecular basis of K+ conduction and selectivity. *Science*, *280*, 69-77.

Dubowy, C. & Sehgal, A. (2017). Circadian rhythms and sleep in *Drosophila melanogaster*. *Genetics*, *205*, 1373-1397.

Esterbauer, H., Schaur, R. J. & Zollner, H. (1991). Chemistry and biochemistry of 4-hydroxynonenal, malonaldehyde and related aldehydes. *Free Radic Biol Med*, *11*, 81-128.

Faivre, J. F., Calmels, T. P., Rouanet, S., Javre, J. L., Cheval, B. & Bril, A. (1999). Characterisation of Kv4.3 in HEK293 cells: comparison with the rat ventricular transient outward potassium current. *Cardiovasc Res*, *41*, 188-199.

Gault, J., Liko, I., Landreh, M., Shutin, D., Bolla, J. R., Jefferies, D., Agasid, M., Yen, H., Ladds, M. J. G. W., Lane, D. P., Khalid, S., Mullen, C., Remes, P. M., Huguet, R., McAlister, G., Goodwin, M., Viner, R., Syka, J. E. P. & Robinson, C. V. (2020). Combining native and 'omics' mass spectrometry to identify endogenous ligands bound to membrane proteins. *Nat Methods*, *17*, 505-508.

González, C., Baez-Nieto, D., Valencia, I., Oyarzún, I., Rojas, P., Naranjo, D. & Latorre R. (2012). K(+) channels: function-structural overview. *Compr Physiol*, *2*, 2087-2149.

Gulbis, J. M., Mann, S. & MacKinnon, R. (1999). Structure of a voltage-dependent K+ channel β subunit. *Cell*, *97*, 943-952.

Gulbis, J. M., Zhou, M., Mann, S. & MacKinnon R. (2000). Structure of the cytoplasmic β subunit-T1 assembly of voltage-dependent K+ Channels. *Science*, *289*, 123-127.

Guo, F., Holla, M. Diaz, M. M. & Rosbash, M. (2018). A circadian output circuit controls sleep-wake arousal in Drosophila. *Neuron*, *100*, 624-635.

Guo, F., Yu, J., Jung, H. J., Abruzzi, K. C., Luo, W., Griffith, L. C., & Rosbash, M. (2016). Circadian neuron feedback controls the Drosophila sleep-activity profile. *Nature*, *536*, 292-297.

Guo, W., Li, H., London, B. & Nerbonne, J. M. (2000). Functional consequences of elimination of i(to,f) and i(to,s): early afterdepolarizations, atrioventricular block, and ventricular arrhythmias in mice lacking Kv1.4 and expressing a dominant-negative Kv4 alpha subunit. *Circ Res.*, *87*, 73-79.

Higdon, A., Diers, A. R., Oh, J. Y., Landar, A., & Darley-Usmar, V. M. (2012). Cell signalling by reactive lipid species: new concepts and molecular mechanisms. *The Biochemical journal*, *442*, 453–464.

Hill, V. M., O'Connor, R. M., Sissoko, G. B., Irobunda, I. S., Leong, S., Canman, J. C., Stavropoulos, N. & Shirasu-Hiza, M. (2018). A bidirectional relationship between sleep and oxidative stress in Drosophila. *PLoS Biol*., *16*, e2005206.

Hoog, S. S., Pawlowski, J. E., Alzari, P. M., Penning, T. M., & Lewis, M. (1994). Three-dimensional structure of rat liver 3 alpha-hydroxysteroid/dihydrodiol dehydrogenase: a member of the aldo-keto reductase superfamily. *Proceedings of the National Academy of Sciences of the United States of America*, *91*, 2517–2521.

Hoshi, T. Zagotta, W. N. & Aldrich R. W. (1990). Biophysical and molecular mechanisms of Shaker potassium channel inactivation. *Science*, *250*, 533-538.

Hu, W., Peng, Y., Sun, J., Zhang, F., Zhang, X., Wang, L., Li, Q. & Zhong, Y. (2018). Fan-shaped body neurons in the Drosophila brain regulate both innate and conditioned nociceptive avoidance. *Cell Rep*, *24*, 1573-1584.

Hulse, B. K., Haberkern, H., Franconville, R., Turner-Evans, D. B., Takemura, S., Wolff, T., Noorman, M., Dreher, M., Dan, C., Parekh, R., Hermundstad, A. M., Rubin, G. & Jayaraman, V. (2021). A connectome of the *Drosophila* central complex reveals network motifs suitable for flexible navigation and context-dependent action selection. *Elife*, *10*, e66039.

Jakubcakova, V., Curzi, M. L., Flachskamm, C., Hambsch, B., Landgraf, R. & Kimura, M. (2013). The glycolytic metabolite methylglyoxal induces changes in viligance by generating low-amplitude non-REM sleep. *J Psychopharmacol.*, *27*, 1070-1075.

Jan, L. Y. & Jan, Y. N. (2012). Voltage-gated potassium channels and the diversity of electrical signaling. *J Physiol*, *590*, 2591-2599.

Jiang, B., Sun, X., Cao, K. & Wang, R. (2002). Endogenous Kv channels in human embryonic kidney (HEK-293) cells. *Mol Cell Biochem*, *238*, 69-79.

Joiner, W. J. (2016). Unraveling the evolutionary determinants of sleep. *Curr Biol*, *26*, R1073–R1087.

Kacsoh, B. Z., Bozler, J., Hodge, S. & Bosco, G. (2019). Neural circuitry of social learning in Drosophila requires multiple inputs to facilitate inter-species communication. *Commun Biol*, *2.*

Kelley, L. A., Mezulis, S., Yates, C. M., Wass, M. N. & Sternberg, M. J. E. (2015). The Phyre2 web portal for protein modeling, prediction and analysis. *Nat Protoc*, *10*, 845-858.

Kempf, A., Song, S. M., Talbot, C. B. & Miesenböck, G. (2019). A potassium channel β-subunit couples mitochondrial electron transport to sleep. *Nature*, *568*, 230-234.

King, A. N. & Sehgal, A. (2020). Molecular and circuit mechanisms mediating circadian clock output in the Drosophila brain. *Eur J Neurosci*, *51*, 268-281.

Krump, C., Vogl, M., Brecker, L., Nidetzky, B. & Kratzer, R. (2014). Acceleration of an aldo-keto reductase by minimal loop engineering. *Protein Eng Des Sel*, *27*, 245-248.

Lai, H. C. & Jan, L. Y. (2006). The distribution and targeting of neuronal voltage-gated ion channels. *Nat Rev Neurosci*, *7*, 548-562.

Lamaze, A., Kratschmer, P., Chen, K. F., Lowe, S. & Jepson, J. E. C. (2018). A wake-promoting circadian output circuit in Drosophila. *Curr Biol*, *28*, 3098-3105.

Li, F., Liu, J., Zheng, Y., Garavito, R. M. & Ferguson-Miller, S. (2015). Crystal structures of translocator protein (TSPO) and mutant mimic of a human polymorphism. *Science*, *347*, 555-558.

Lin, D., Lee, H., Liu, Q., Perry, G., Smith, M. A. & Sayre, L. M. (2005). 4-Oxo-2-nonenal is both more neurotoxic and more protein reactive than 4-hydroxy-2-nonenal. *Chem Res Toxicol*, *18*, 1219-1231.

Liu, S., Liu, Q., Tabuchi, M. & Wu, M. N. (2016). Sleep drive is encoded by neural plastic changes in a dedicated circuit. *Cell*, *165*, 1347-1360.

Liu, S. Q., Jin, H., Zacarias, A., Srivastava, S. & Bhatnagar, A. (2001). Binding of pyridine nucleotide coenzymes to the beta-subunit of the voltage-sensitive K+ channel. *J Biol Chem*, *276*, 11812-11820.

Liu, X., Wang, C., Zhang, L., Yao, Z., Cui, D., Wu, L., Lin, J., Yuan, Y. A. & Wei, D. (2014). Structural and mutational studies on an aldo-keto reductase AKR5C3 from *Gluconobacter oxydans*. *Protein Sci*, *23*, 1540-1549.

Long, S. B., Campbell, E. B. & MacKinnon, R. (2005). Crystal structure of a mammalian voltage-dependent *Shaker* family K+ channel. *Science*, *309*, 897-903.

Lyons, D. G. & Rihel, J. (2020). Sleep Circuits and Physiology in Non-Mammalian Systems. *Current opinion in physiology*, *15*, 245–255.

May-Zhang, L. S., Yermalitsky, V., Melchior, J. T., Morris, J., Tallman, K. A., Borja, M. S., Pleasant, T., Amarnath, V., Song, W., Yancey, P. G., Davidson, W. S., Linton, M. F. & Davies, S. S. (2019). Modified sites and functional consequences of 4-oxo-2-nonenal adducts in HDL that are elevated in familial hypercholesterolemia. *J Biol Chem*, *294*, 19022-19033.

McCormack, K., Connor, J. X., Zhou, L., Ho, L. L., Ganetzky, B., Chiu, S. & Messing A. (2002). Genetic analysis of the mammalian K+ channel β subunit Kvβ2 (*Kcnab2*). *J Biol Chem*, *277*, 13219-13228.

McCormack, T. & McCormack, K. (1994). *Shaker* K+ channel β subunits belong to an NAD(P)H-dependent oxidoreductase superfamily. *Cell*, *79*, 1133-1135.

Mehmood, S., Allison, T. M. & Robinson, C. V. (2015). Mass spectrometry of protein complexes: from origins to applications. *Annu Rev Phys Chem*, *66*, 453-474.

Mignot, E. (2008). Why we sleep: the temporal organization of recovery. *PLoS Biol*, *6*, e106.

Murphy, M. P. (2009). How mitochondria produce reactive oxygen species. *The Biochemical journal*, *417*, 1–13.

Nagata, N. & Urade, Y. (2012). Sleep-wake regulation by prostaglandin D2 and adenosine. *Brain Nerve*, *64*, 621-628.

Nagaya, N., & Papazian, D. M. (1997). Potassium channel alpha and beta subunits assemble in the endoplasmic reticulum. *The Journal of biological chemistry*, *272*, 3022–3027.

Ni, J. D., Gurav, A. S., Liu, W., Ogunmowo, T. H., Hackbart, H., Elsheikh, A., Verdegaal, A. A. & Montell, C. (2019). Differential regulation of the *Drosophila* sleep homeostat by circadian and arousal inputs. *Elife*, *8*, e40487.

Pan, Y., Weng, J., Cao, Y, Bhosle, R. C. & Zhou, M. (2008a). Functional coupling between the K_v1.1 channel and aldoketoreductase $K_v\beta$1. *J Biol Chem*, *283*, 8634-8642.

Pan, Y., Weng, J., Kabaleeswaran, V., Li, H., Cao, Y., Bhosle, R. C. & Zhou, M. (2008b). Cortisone dissociates the Shaker family K+ channels from their beta subunits. *Nat Chem Biol.*, *4*, 708-714.

Parvez, S., Long, M. J. C., Lin, H., Zhao, Y., Haegele, J. A., Pham, V. N., Lee, D. K. & Aye, Y. (2016). T-REX on-demand redox targeting in live cells. *Nat Protoc*, *11*, 2328-2356.

Parvez, S., Long, M. J. C., Poganik, J. R. & Aye, Y. (2018). Redox signaling by reactive electrophiles and oxidants. *Chem Rev*, *118*, 8798-8888.

Pérez, J. M., Arenas, F. A., Pradenas, G. A., Sandoval, J. M. & Vásquez, C. C. (2008). Escherichia coli YqhD exhibits aldehyde reductase activity and protects from the harmful effect of lipid peroxidation-derived aldehydes. *J Biol Chem*, *283*, 7346-7353.

Pimentel, D., Donlea, J. M., Talbot, C. B., Song, S. M., Thurston, A. J. F. & Miesenböck, G. (2016). Operation of a homeostatic sleep switch. *Nature*, *536*, 333–337.

Pongs, O., Leicher, T., Berger, M., Roeper, J., Bähring, R., Wray, D., Giese, K. P., Silva, A. J. & Storm, J. F. (1999). Functional and molecular aspects of voltage-gated K+ channel beta subunits. *Ann N Y Acad Sci, 868*, 344-355.

Qian, Y., Cao, Y., Deng, B., Yang, G., Li, J., Xu, R., Zhang, D., Huang, J. & Rao, Y. (2017). Sleep homeostasis regulated by 5HT2b receptor in a small subset of neurons in the dorsal fan-shaped body of drosophila. *eLife*, *6*.

Raph, S. M., Bhatnagar, A. & Nystoriak, M. A. (2019). Biochemical and physiological properties of K^+ channel-associated AKR6A ($K_v\beta$) proteins. *Chem Biol Interact*, *305*, 21-27.

Rettig, J., Heinemann, S. H., Wunder, F., Lorra, C., Parcej, D. N., Dolly, J. O. & Pongs, O. (1994). Inactivation properties of voltage-gated K+ channels altered by presence of β-subunit. *Nature*, *369*, 289-294.

Robinson, C. V. (2019). Mass spectrometry: From plasma proteins to mitochondrial membranes. *Proc Natl Acad Sci U S A*, *116*, 2814-2820.

Ruppersberg, J. P., Stocker, M., Pongs, O., Heinemann, S. H., Frank, R. & Koenen, M. (1991). Regulation of fast inactivation of cloned mammalian IK(A) channels by cysteine oxidation. *Nature*, *352*, 711-714.

Sakai, T., Inami, S., Sato, S., & Kitamoto, T. (2012). Fan-shaped body neurons are involved in period-dependent regulation of long-term courtship memory in Drosophila. *Learning & memory (Cold Spring Harbor, N.Y.)*, *19*(12), 571–574.

Sakai, T. & Kitamoto, T. (2006). Differential roles of two major brain structures, mushroom bodies and central complex, for Drosophila male courtship behavior. *J Neurobiol*, *66*, 821-834.

Sareen, P. F., McCurdy, L. Y. & Nitabach, M. N. (2021). A neuronal ensemble encoding adaptive choice during sensory conflict in Drosophila. *Nat Commun*, *12*, 4131.

Schlichting, M., Diaz, M. M., Xin, J., & Rosbash, M. (2019). Neuron-specific knockouts indicate the importance of network communication to *Drosophila* rhythmicity. *eLife*, *8*, e48301.

Schwarz, J. E., King, A. N., Hsu, C. T., Barber, A. F. & Sehgal, A. (2021). *Hugin*$^{+}$ neurons provide a link between sleep homeostat and circadian clock neurons. *Proc Natl Acad Sci U S A*, *118*.

Scott, V. E., Muniz, Z. M., Sewing, S., Lichtinghagen, R., Parcej, D. N., Pongs, O. & Dolly, J. O. (1994). Antibodies specific for distinct Kv subunits unveil a heterooligomeric basis for subtypes of alpha-dendrotoxin-sensitive K+ channels in bovine brain. *Biochemistry*, *33*, 1617–1623.

Shi, G., Nakahira, K., Hammond, S., Rhodes, K. J., Schechter, L. E., & Trimmer, J. S. (1996). Beta subunits promote K+ channel surface expression through effects early in biosynthesis. *Neuron*, *16*, 843–852.

Sies, H., & Jones, D. P. (2020). Reactive oxygen species (ROS) as pleiotropic physiological signalling agents. *Nature reviews. Molecular cell biology*, *21*(7), 363–383.

Smart, O. S., Horsky, V., Gore, S., Varekova, R. S., Bendova, V., Kleywegt, G. J. & Velankar, S. (2018). Validation of ligands in macromolecular structures determined by X-ray crystallography. *Acta Crystallogr D Struct Biol*, *74*, 228-236.

Strauss, R. (2002). The central complex and the genetic dissection of locomotor behaviour. *Curr Opin Neurobiol*, *12*, 633-638.

Tabuchi, M., Monaco, J. D., Duan, G., Bell, B., Liu, S., Liu, Q., Zhang, K. & Wu, M. N. (2018). Clock-generated temporal codes determine synaptic plasticity to control sleep. *Cell*, *175*, 1213-1227.

Tan, X., Bae, C., Stix, R., Fernandez-Marino, A. I., Huffer, K., Chang, T., Jiang, J., Feraldo-Gomez, J. D. & Swartz, K. J. (2022). Structure of the Shaker Kv channel and mechanism of slow C-type inactivation. *Sci Adv*, *18*, 7814.

Tipparaju, S. M., Barski, O. A., Srivastava, S. & Bhatnagar, A. (2008). Catalytic mechanism and substrate specificity of the β-subunit of the voltage-gated potassium channel. *Biochemistry*, *47*, 8840-8854.

Tur, J., Chapalamadugu, K. C., Katnik, C., Cuevas, J., Bhatnagar, A. & Tipparaju, S. M. (2017). $K_v\beta1.1$ (AKR6A8) sense pyridine nucleotide changes in the mouse heart and modulates cardiac electrical activity. *Am J Physiol Heart Circ Physiol.*, *312*, H571-H583.

Ueda, A. & Wu, C. (2008). Effects of hyperkinetic, a beta subunit of Shaker voltage-dependent K+ channels, on the oxidation state of presynaptic nerve terminals. *J Neurogenet*, *22*, 1-13.

Ueno, T. Tomita, J, Tanimoto, H. Endo, K., Ito, K., Kume, S. & Kume, K. (2012). Identification of a dopamine pathway that regulates sleep and arousal in Drosophila. *Nat Neurosci*, *15*, 1516-1523.

Urade, Y. & Hayaishi, O. (2011). Prostaglandin D2 and sleep/wake regulation. *Sleep Med Rev.*, *15*, 411-418.

Wang, Q., Ye, T., Ma, Z., Chen, R., Xie, T. & Yin, X. (2014). Characterization and site-directed mutation of a novel aldo-keto reductase from *Lodderomyces*

elongisporus NRRL YB-4239 with high production rate of ethyl (R)-4-chloro-3-hydroxybutanoate. *J Ind Microbiol Biotechnol*, *41*, 1609-1616.

Weir, P. T. & Dickinson, M. H. (2015). Functional divisions for visual processing in the central brain of flying Drosophila. *Proc Natl Acad Sci U S A*, *112.*

Weng, J., Cao, Y., Moss, N. & Zhou, M. (2006). Modulation of voltage-dependent *Shaker* family potassium channels by an aldo-keto reductase. *J Biol Chem*, *281*, 15194-15200.

Wetzels, S., Wouters, K., Schalkwijk, C. G., Vanmierlo, T. & Hendriks, J. J. A. (2017). Methylglyoxal-derived advanced glycation endproducts in multiple sclerosis. *Int J Mol Sci*, *18*, 421.

Wolff, T, Iyer, N. A., & Rubin, G. M. (2015). Neuroarchitecture and neuroanatomy of the *Drosophila* central complex: a GAL4-based dissection of protocerebral bridge neurons and circuits. *Journal of Comparative Neurology*, *523*, 997-1037.

Wong, H. S., Benoit, B., & Brand, M. D. (2019). Mitochondrial and cytosolic sources of hydrogen peroxide in resting C2C12 myoblasts. *Free radical biology & medicine*, *130*, 140–150.

Xie, Z., Barski, O. A., Cai, J., Bhatnagar, A. & Tipparaju, S. M. (2011). Catalytic reduction of carbonyl groups in oxidized PAPC by $K_v\beta2$ (AKR6). *Chem Biol Interact*, *191*, 255-260.

Xu, P., Cox, K. H., & Takahashi, J. S. (2019). A Hyperkinetic Redox Sensor Drives Flies to Sleep. *Trends in neurosciences*, *42*, 514–517.

Zagotta, W. N., Hoshi, T. & Aldrich, R. W. (1990). Restoration of inactivation in mutants of Shaker potassium channels by a peptide derived from ShB. *Science*, *250*, 568-571.